Bioelectrochemistry 166 (2025) 109043

Contents lists available at ScienceDirect

Bioelectrochemistry

journal homepage: www.journals.elsevier.com/bioelectrochemistry

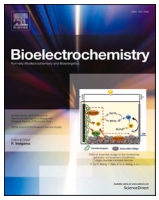

Acoustic streaming on antibody-functionalized screen-printed electrode enhances detection sensitivity and total assay duration for voltammetric immunosensing of newcastle disease virus

Mohamad Farid Abd Muain [a,b], Amir Syahir Amir Hamzah [a,b,d], Suet Lin Chia [c,g,h], Khatijah Yusoff [c,h], Hong Ngee Lim [e], Shinya Ikeno [f], Thomas Laurell [i], Asilah Ahmad Tajudin [a,b,c,*]

[a] Nanobiotechnology Research Group, Faculty of Biotechnology and Biomolecular Sciences, Universiti Putra Malaysia, 43400 UPM, Serdang, Selangor Darul Ehsan, Malaysia
[b] Laboratory of Virology, Faculty of Biotechnology and Biomolecular Sciences, Universiti Putra Malaysia, 43400 UPM, Serdang, Selangor Darul Ehsan, Malaysia
[c] Department of Microbiology, Faculty of Biotechnology and Biomolecular Sciences, Universiti Putra Malaysia, 43400 UPM, Serdang, Selangor Darul Ehsan, Malaysia
[d] Department of Biochemistry, Faculty of Biotechnology and Biomolecular Sciences, Universiti Putra Malaysia, 43400 Serdang, Selangor, Malaysia
[e] Department of Chemistry, Faculty of Science, Universiti Putra Malaysia, 43400 Serdang, Selangor, Malaysia
[f] Department of Biological Functions Engineering, Graduate School of Life Science and System Engineering, Kyushu Institute of Technology, Kitakyushu Science and Research Park, Kitakyushu, Fukuoka, Japan
[g] UPM-MAKNA Cancer Research Laboratory, Institute of Bioscience, Universiti Putra Malaysia, 43400 UPM, Serdang, Selangor, Malaysia.
[h] Malaysia Genome & Vaccine Institute, National Institutes of Biotechnology Malaysia, Jalan Bangi, 43000 Kajang, Selangor, Malaysia
[i] Department of Biomedical Engineering, Faculty of Engineering, Lund University, Box 117, 22100 Lund, Sweden

ARTICLE INFO

Keywords:
Acoustic streaming
Piezoelectric
Micromixing
Electrochemical immunosensor

ABSTRACT

Conventional diagnostic methods often involve long incubation times due to limited fluid mixing in confined spaces, despite offering high sensitivity. Therefore, acoustic streaming was employed to enhance microscale advection, thereby improving biomolecular interactions and reducing assay duration. The micromixing capability was demonstrated by dispersing methylene blue (MB) in deionized water and glycerol solutions, where homogenization time decreased by approximately 80 % in water and 84–88 % in glycerol under acoustic actuation. Biomolecule adsorption was modeled using MB adsorbed onto cellulose acetate–graphene oxide (CA-GO) beads, showing improved adsorption and a reduced time to saturation from 16 to 8 min. Maximum adsorption occurred at 2 MHz frequency and 20 V amplitude. By using these optimized parameters, voltammetric immunosensing of Newcastle disease virus (NDV) was performed on PEG-alkanethiol-modified screen-printed gold electrodes (SPGE). The system incorporating acoustic streaming was compared against one without it. Results demonstrated a comparable limit of detection (1.46 HA μL^{-1} at 3σ m^{-1}) achieved at shorter assay duration (8 min). These findings underscore the potential of acoustic streaming in electrochemical immunosensors to accelerate diagnostic assays without compromising sensitivity or specificity, particularly for applications utilizing screen-printed electrodes.

1. Introduction

Disease diagnostics and pathogen detection play a critical role in the early identification of infections, facilitating timely interventions to control disease spread and enabling the monitoring of disease progression [1,2]. Conventional diagnostic techniques including molecular methods such as polymerase chain reaction (PCR) and real-time PCR [3], enzyme-linked immunosorbent assay (ELISA) [4] and

* Corresponding author at: Nanobiotechnology Research Group, Faculty of Biotechnology and Biomolecular Sciences, Universiti Putra Malaysia, 43400 UPM, Serdang, Selangor Darul Ehsan, Malaysia.
E-mail addresses: gs55497@student.upm.edu.my (M.F. Abd Muain), amirsyahir@upm.edu.my (A.S. Amir Hamzah), suetlin@upm.edu.my (S.L. Chia), kyusoff@upm.edu.my (K. Yusoff), hongngee@upm.edu.my (H.N. Lim), ikeno@life.kyutech.ac.jp (S. Ikeno), thomas.laurel@bme.lth.se (T. Laurell), asilah_at@upm.edu.my (A. Ahmad Tajudin).

https://doi.org/10.1016/j.bioelechem.2025.109043
Received 6 June 2025; Received in revised form 3 July 2025; Accepted 6 July 2025
Available online 7 July 2025

immunofluorescence [5] have been employed. Even though these methods are recognized for their sensitivity, they suffer from the problems such as being labor intensive and having long sample-to-answer duration [6]. For instance, ELISA is typically limited by diffusion-driven kinetics, resulting in lengthy sample incubation periods [7]. Additional limitations include the need for large sample volumes and low surface-to-volume ratios, which hinder their suitability for rapid and sensitive disease and pathogen detection [1].

Electrochemical detection approaches offer a promising alternative due to their operational simplicity, high sensitivity, rapid response times, portability, and potential for miniaturization [8,9]. These characteristics are advantageous for point-of-care diagnostics that require swift detection of target analytes, thereby improving disease management and enabling prompt medical decisions [10]. Moreover, the portability of electrochemical immunosensors supports decentralized clinical testing, allowing for in situ diagnostics [11,12].

A key limitation of conventional diagnostic methods is the extended incubation time caused by diffusion-limited analyte transport [13]. In order to overcome this problem, both passive and active micromixing strategies can be integrated into sample incubation systems, particularly in microfluidic platforms where fluids operate at the microscale [14]. Passive micromixers rely on channel geometry modifications to induce mixing without external energy input [14,15]. In contrast to passive micromixers, active micromixers utilize external stimuli such as thermal [16], electric [17], pressure [18] and magnetic [19] fields, as well as acoustic perturbation [20] to induce the fluid mixing [21]. Among them, acoustic-induced micromixing or acoustofluidics is particularly attractive due to its biocompatibility and applicability to a wide range of liquid viscosities [22]. Besides that, acoustofluidics does not require labelling of liquid samples as in electric- or magnetic-based methods, [23].

Acoustofluidics has been widely adopted in various biological applications for its ability to manipulate biomolecules and nanoparticles, enabling mixing [24], patterning [25], focusing and enrichment [26], separation [27], sorting [28], entrapment [29], and cell lysis [23]. Besides that, acoustofluidic also has been applied in the development of biosensors [30]. For example, Li et al. [31] applied acoustofluidics to enrich target analytes at the sensing surface, enhancing sensitivity while reducing incubation time. Similarly, Syamila et al. [32] employed acoustic streaming generated by a piezoelectric plate coupled to a screen-printed carbon electrode (SPCE), improving mass transfer of analytes to the bioreceptor layer and shortening assay duration due to mechanical vibration. Such reduction in incubation time is desirable for point-of-care devices that require fast and efficient analyte detection [33,34]. In addition to SPCEs, acoustic streaming has also been demonstrated with materials like polystyrene [13], paper [35], polydimethylsiloxane (PDMS) [36] and polymethyl methacrylate (PMMA) [37].

Another crucial challenge in biosensor development is biofouling, wherein non-specific protein adsorption occurs on the bioreceptor-functionalized surface, compromising sensitivity and specificity [38]. Mitigation strategies involve either passive or active antifouling approaches [39]. Passive methods typically involve coating the sensing surface with blocking layers using proteins such as bovine serum albumin [40] and milk proteins [41], or the formation of hydrophilic layer by polyethylene glycols [42] and zwitterionic polymers [43]. Active methods rely on mechanical or acoustic vibrations or pressure-driven flows to prevent non-specific protein adsorption [39]. For instance, Pan et al. [44] utilized acoustic streaming to generate microvortexes in the sample solution, facilitating the removal of non-specific proteins from the sensor surface.

This study demonstrates that acoustic streaming induced from a vibrating piezoelectric plate that was placed under the screen-printed electrode has improved micromixing in a small volume of liquid sample that was applied to the sensor surface. While the fundamental characterization of acoustic streaming such as flow pattern visualization, acoustic pressure distribution in fluids, and the manipulation of micro- and nanoparticles has been well-documented in previous literature [45,46], this study focuses on harnessing the effect to enhance sample mixing and, in turn, improve the analytical performance of an electrochemical immunosensor targeting a viral analyte. Firstly, methylene blue (MB) dye was dispersed in water droplets and glycerol droplets with varied viscosity to evaluate the improvement of micromixing by the induced acoustic streaming. Secondly, adsorption of MB dye onto cellulose acetate-graphene oxide (CA-GO) was studied with and without acoustic streaming to evaluate the improvement of biomolecules adsorption at different incubation duration, as well as at different actuation frequencies and amplitudes. Subsequently, the detection of Newcastle disease virus (NDV) was studied in the presence of acoustic streaming to monitor its improved adsorption onto NDV-specific polyclonal antibodies (anti-NDV) that were immobilized on screen-printed gold electrodes (SPGE). The sensitivity, specificity and selectivity studies of NDV detection were also carried out, as well as the detection of NDV in diluted allantoic fluid as a real sample candidate.

2. Experimental

2.1. Materials and instrumentation

NDV LaSota strain and rabbit polyclonal anti-NDV were obtained from the Virology Laboratory, Faculty of Biotechnology and Biomolecular Sciences, Universiti Putra Malaysia. Carboxy-polyethylene glycol-undecanethiol (CEGU, IUPAC name: 20-(11-mercaptoundecanyloxy)-3,6,9,12,15,18-hexaoxaeicosanoic acid) for SAM formation on SPGE was purchased from Dojindo Laboratories (Kumamoto, Japan). 1-Ethyl-3-(3′-dimethylaminopropyl)carbodiimide hydrochloride (EDC•HCl) was purchased from Beijing Solarbio Science & Technology Co., Ltd. (Beijing, China). Dimethyl sulfoxide (DMSO) and undenatured absolute ethanol were purchased from Merck (Massachusetts, USA). Cellulose acetate (CA), potassium hexacyanoferrate(III) ($K_3Fe(CN)_6$) powder, ammonia solution (25 %), N-hydroxysuccinimide sodium salt (NHS) and acetic acid solution (100 %) were purchased from Sigma-Aldrich (Missouri, USA). Both SPGE and SPCE were purchased from Metrohm Dropsens (Parque Technologico de Asturias, Spain). Ultrasonic gel was purchased from Parker Laboratories Inc. (New Jersey, USA). Electrochemical measurement was done on Metrohm 910 PGSTAT mini (Herisau, Switzerland) portable potientiostat. Deionized water (dH_2O) was obtained from Elga Purelab Classic water purification system (Illinois, USA) where the resistivity was at least 18.2 MΩ.cm.

2.2. NDV propagation and clarification

NDV propagation and clarification procedures were adapted from previous study [47]. Briefly, NDV suspension (20 HA, 100 μL in PBS) has been inoculated in 9-day old specific pathogen free (SPF) embryonated chicken eggs. Incubation of NDV-inoculated eggs were done in a humidified incubator at 37 °C for 2 days. The eggs were then transferred into a chiller (4 °C) for 1 h. Next, allantoic fluid that contains NDV was clarified by opening the air sac of chicken embryo by using a sterilized spatula. The allantoic fluid was then aseptically transferred into sterile 50-mL centrifuge tubes and centrifuged twice at 8000 rpm (7741 ×*g*, 4 °C) for 10 min to remove any cellular debris, and once at 20000 rpm (48,384 ×*g*, 4 °C) for 4 h to pellet the NDV. The pellet was resuspended in PBS (50 mM, pH 7) and subsequently tested using the HA assay to determine the stock NDV concentration. From the HA assay that was run in triplicate, it was determined that the stock concentration of NDV suspension to be at 64 HA μL^{-1}.

2.3. Evaluation of micromixing induction by acoustic streaming through dispersion of MB dye in water droplet

The induction of micromixing through acoustic streaming actuation

was adapted from previous studies [48,49]. Firstly, the apparatus needed for the study was assembled as shown in Fig. 1(A), where SPCE was placed directly on the lab bench surface for the incubation without acoustic streaming, and a separate SPCE was temporarily affixed to a piezoelectric plate using ultrasonic gel and supported by a holder, as shown in Fig. 1(B). Subsequently, dH_2O (39 μL) and MB (1 %, 1 μL) were dropped onto the working electrode of the SPCE, representing micromixing induction on a carbon-based screen-printed electrode. By continuously observing the dispersion of MB in the liquid droplet using naked eyes and a magnifying glass, the time required for the MB dye to disperse homogeneously within the dH_2O droplet was then measured and recorded in triplicate under two incubation conditions, i.e., with and without acoustic actuation from a piezoelectric plate placed beneath the SPCE. Acoustic streaming actuated by piezoelectric was applied at the frequency of 2 MHz and an amplitude of 20 V. The study was repeated using SPGE and silver-electrodeposited SPCE (SPCE/Ag) to represent a metal-based screen-printed electrode and metal nanoparticle-electrodeposited screen-printed electrode, respectively. Additionally, the dH_2O droplet was replaced with glycerol at varying concentrations to assess micromixing efficiency in viscous liquids. All incubation procedures were conducted at room temperature.

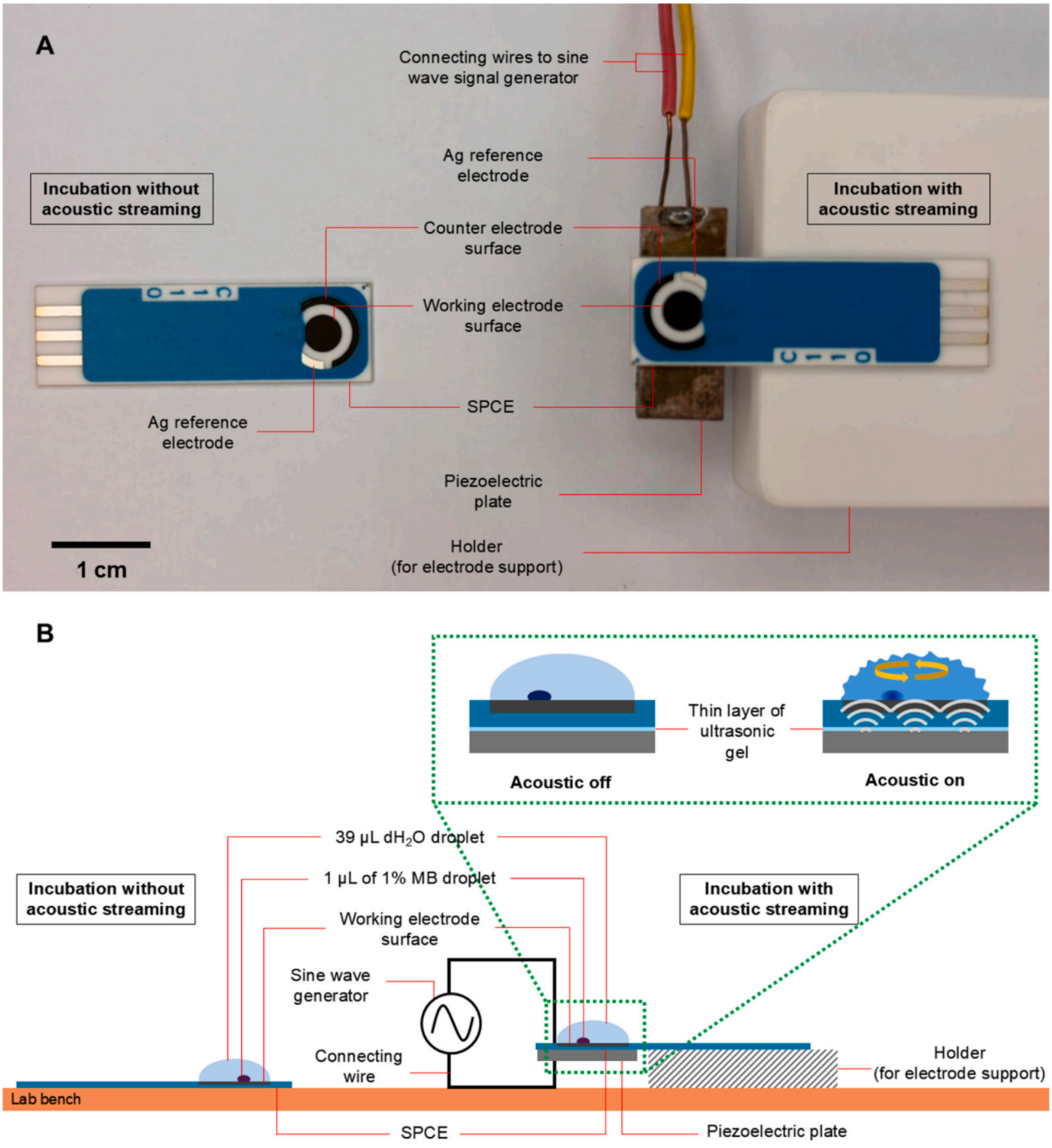

Fig. 1. Experimental set up for evaluation of micromixing induction by acoustic streaming through dispersion of MB dye in water droplet. (A) Photograph of actual set up of experiment. (B) Schematic diagram of MB mixing in liquid droplet on SPCE working electrode. SPCE was placed directly on the lab bench for incubation without acoustic streaming, whereas another SPCE was placed on a piezoelectric plate by temporarily fixing with ultrasonic gel for incubation with acoustic streaming. SPCE was later replaced with SPGE and SPCE/Ag, and dH_2O droplet was replaced with glycerol droplets with varied concentrations.

2.4. Fabrication of CA-GO beads

CA-GO beads fabrication methodology was adapted from the previous study done by Eltaweil et al. [50]. Firstly, CA (1 g) was dissolved in DMSO (5 mL) by using magnetic stirrer for 30 min in a beaker, while GO (10 % *w/v*) was dispersed in DMSO (5 mL) by using ultrasonic waterbath for 30 min in a separate beaker. After that, GO suspension was gradually added into CA solution while being stirred vigorously for 30 min. Next, the CA-GO composite solution was dispensed drop by drop into distilled H_2O (250 mL) using a syringe to form the beads. These beads were then left (15 min) to cure before being collected and thoroughly washed with distilled H_2O.

2.5. Evaluation of adsorption by using acoustic streaming through the adsorption of MB dye on CA-GO beads

The evaluation was adapted from previous studies [51,52] with modifications. A similar experimental setup was employed as described previously in Fig. 1 (Section 2.3), except that the dH_2O (39 μL) and MB (1 %, 1 μL) were replaced with MB solution (100 mg L^{-1}, 40 μL) and CA-GO beads, respectively. Firstly, dried CA-GO beads with a total weight of 4 mg, were placed and arranged on the SPCE working electrode surface. Subsequently, MB (100 mg L^{-1}, 40 μL) solution was added to the same electrode surface, fully submerging the CA-GO beads. Next, the sine wave signal generator was activated with an AC frequency of 2 MHz and an amplitude of 20 V to initiate acoustic actuation from the piezoelectric plate. The adsorption of MB onto the CA-GO beads was allowed to proceed for 1 to 16 min. After incubation, the remaining MB solution was removed using a micropipette. The resulting beads, referred to as CA-GO/MB, were then washed twice with dH_2O (40 μL) to eliminate any excess MB dye from the electrode surface. The CA-GO/MB beads were subsequently fixed onto the SPCE working electrode surface using PVDF (5 %, 2 μL) solution. All steps were repeated under vibration-free condition on a laboratory bench to incubate the MB solution with CA-GO beads without acoustic streaming. Finally, all electrodes with fixed CA-GO/MB were subjected to electrochemical characterization via cyclic voltammetry (CV) analysis to evaluate the improvement in beads conductivity following MB adsorption. The CV was performed within a potential window of −1.0 to 1.0 V, at a scan rate of 50 mV s^{-1}, using an electrolyte solution containing $Fe(CN)_6^{3-/4-}$ (5 mM) as the redox probe in KCl (0.1 M) as the supporting electrolyte. The adsorption of MB onto CA-GO beads was run in triplicate. Next, the anodic peak changes (ΔI_{pa}) and cathodic peak changes (ΔI_{pc}) from CV analysis were calculated as described in Eq. 1 and Eq. 2, respectively.

$$\Delta I_{pa} = \left(I_{pa\ CA-GO} - I_{pa\ CA-GO/MB}\right)/I_{pa\ CA-GO}\ \text{x}\ 100 \quad (1)$$

$$\Delta I_{pc} = \left(I_{pc\ CA-GO} - I_{pc\ CA-GO/MB}\right)/I_{pc\ CA-GO}\ \text{x}\ 100 \quad (2)$$

where, $I_{pa\ CA\text{-}GO}$ and $I_{pc\ CA\text{-}GO}$ are I_{pa} and I_{pc} values that were produced by bare CA-GO fixed on the electrode, while $I_{pa\ CA\text{-}GO/MB}$ and $I_{pc\ CA\text{-}GO/MB}$ are I_{pa} and I_{pc} that produced by CA-GO/MB fixed on the electrode.

2.6. Applicability of acoustic streaming in improving the sensing of NDV through direct detection immunoassay

2.6.1. Fabrication of NDV sensing electrode

The fabrication method for this sensing platform was adapted from a previous study [53] with modifications. Firstly, the SPGE was thoroughly cleaned with dH_2O and air-dried. Next, the working electrode surface of the SPGE was modified with a self-assembled monolayer (SAM). This was done by overnight incubation of ethanolic CEGU (1 mM, 20 μL) solution at room temperature. After the incubation period, the SPGE was rinsed with undenatured absolute ethanol (5 mL), followed by dH_2O (5 mL), and then air-dried. The resulting electrode now be referred to as SPGE/CEGU. The SPGE/CEGU was subsequently incubated with a carboxyl groups activation solution (20 μL) containing EDC•HCl (0.2 M) and NHS (0.1 M). The incubation lasted for 1 h at room temperature. Then, the electrode was rinsed with dH_2O (5 mL) and air-dried and referred to as SPGE/CEGU/EDC:NHS electrode. For the optimization of anti-NDV as a bioreceptor, anti-NDV (10 μL) at different concentrations (10 to 1000 ng μL^{-1}) was incubated on the SPGE/CEGU/EDC:NHS electrode for 1.5 h in an ice bath. Following the anti-NDV incubation, the electrode was rinsed with dH_2O (5 mL) and air-dried. After determining the optimal concentration of anti-NDV to be used as bioreceptor, the electrode was referred to as SPGE/CEGU/EDC:NHS/anti-NDV. The fabrication of anti-NDV-functionalized platform was completed by incubating the SPGE/CEGU/EDC:NHS/anti-NDV electrode with BSA (3 %, 10 μL) to block the free and empty spaces for binding on the electrode, where the incubation was carried out under the same conditions as the anti-NDV incubation. The completed electrode was referred to as SPGE/CEGU/EDC:NHS/anti-NDV/BSA. The finalized SPGE/CEGU/EDC:NHS/anti-NDV/BSA biosensors were analyzed electrochemically through differential pulse voltammetry (DPV) analysis in an electrolyte solution comprising of $K_3Fe(CN)_6$ (0.1 M, 100 μL) as redox probe and ammonium acetate buffer (pH 4, 1 mL) as supporting electrolyte in dH_2O (10 mL), at potential window of −0.3 to 0.4 V, pulse potential of 10 ms and scan rate of 20 mV s^{-1}. All experiments were done in triplicate.

2.6.2. Detection of NDV on fabricated sensing platform

NDV solution (0.156 to 20 HA μL^{-1} in PBS, 10 μL) was incubated on the SPGE/CEGU/EDC:NHS/anti-NDV/BSA biosensors for 20 min at room temperature, for incubation without acoustic streaming. For incubation with the application of acoustic streaming, the optimum parameters of acoustic streaming (incubation time, and acoustic actuation frequency and amplitude) from adsorption of MB onto CA-GO beads study were used in the incubation of NDV on SPGE/CEGU/EDC:NHS/anti-NDV/BSA biosensors. Subsequently, the electrodes were rinsed with dH_2O (5 mL) and air-dried before electrochemical characterization via DPV as described in Section 2.6.1. Next, the ΔI_{pa} from DPV analysis were calculated as described in Eq. 3.

$$\Delta I_{pa} = \left(I_{pa\ bioreceptor} - I_{pa\ target}\right)/I_{pa\ bioreceptor}\ \text{x}\ 100 \quad (3)$$

where $I_{pa\ bioreceptor}$ is I_{pa} value that produced by SPGE/CEGU/EDC:NHS/anti-NDV/BSA, biosensors while $I_{pa\ target}$ is the I_{pa} that produced after the formation of immunocomplex between anti-NDV and NDV on the electrode surface. After that, Langmuir adsorption isotherm (Eq. 4) has been used to fit the plot of ΔI_{pa} against NDV concentration and to determine the binding adsorption or Langmuir constant (K_L) between anti-NDV and NDV at different concentrations [47].

$$\Delta I_{pa} = \Delta I_{pa\ max}\, K_L\, [\text{NDV}]/(1 + K_L\, [\text{NDV}]) \quad (4)$$

where, [NDV] and $\Delta I_{pa\ max}$ is the concentration of NDV, and maximum ΔI_{pa} produced from the immunocomplex formation between immobilized anti-NDV and NDV at different concentrations, respectively.

2.6.3. Selectivity and specificity study of NDV sensing platform

NDV in PBS (20 HA μL^{-1}, 10 μL) as positive control, and NDV in 1:1000 diluted allantoic fluid (20 HA μL^{-1}, 10 μL) as test sample was allowed to be incubated on the SPGE/CEGU/EDC:NHS/anti-NDV/BSA biosensors, separately with and without acoustic streaming application. After that, the electrodes were rinsed with dH_2O (5 mL) and air dried prior to electrochemical characterization by DPV as described in Section 2.6.2. The ΔI_{pa} was then calculated as in Eq. 3.

2.6.4. Detection of NDV in diluted allantoic fluid

NDV was spiked into 1:1000 diluted allantoic fluid for real sample analysis. This was done as allantoic fluid in embryonated chicken eggs was used for NDV viral isolation, as recommended by the World Organization for Animal Health. In this method, clarified supernatants from

tissue suspensions or feces swabs are inoculated into the allantoic cavity of nine- to eleven-day-old embryonated chicken eggs. Then, the allantoic fluid was harvested and analyzed through the hemagglutination (HA) assay for viral detection and quantification [54].

Each prepared concentration (0.156 to 20 HA μL^{-1}) was incubated (10 μL) on the fabricated SPGE/CEGU/EDC:NHS/anti-NDV/BSA biosensors, separately with and without acoustic streaming application. Following that, the electrodes were rinsed with dH_2O (5 mL) and air-dried before electrochemical characterization via DPV as described in Section 2.6.2. Then, ΔI_{pa} was calculated as in Eq. 3. The relative standard deviation (RSD) values for each concentration of NDV incubated were calculated to compare the ΔI_{pa} values obtained from the detection of NDV spiked in 1:1000 diluted allantoic fluid with those from the control (NDV spiked in PBS, as described in Section 2.6.2).

3. Results and discussion

3.1. Evaluation of micromixing induced by acoustic streaming through dispersion of MB dye in water droplet

The micromixing induced by acoustic streaming was evaluated by dispersion of MB dye in dH_2O droplet. Based on the time required for MB dye to disperse and achieve homogeneity in dH_2O (0 % glycerol, Fig. 2), it was found that the application of acoustic streaming successfully reduced the mixing time needed by approximately 80 %. Notably, regardless of the incubation method, whether with or without acoustic streaming, the time required for MB and dH_2O to reach homogeneity was nearly identical across all three tested electrodes (Fig. S1). For instance, the average time needed for MB to homogenously disperse in dH_2O is 232 s, compared to just 46 s with acoustic streaming, for all electrodes (SPCE, SPGE, and SPCE/Ag). This observation suggested that the electrode surface material did not influence the dispersion or mixing of the sample, indicating that the enhancement in mixing was solely attributed to the application of acoustic streaming. From another perspective, acoustic streaming can be universally applied to various electrode surface materials to enhance mixing efficiency, thus reducing the mixing time in the development of electrochemical biosensors.

Specimen collection for disease diagnostics is usually performed using both non-invasive and invasive methods, such as extraction of body fluids [55,56] and tissue biopsies [57]. For example, various specimens have been used in the diagnosis of COVID-19 including saliva, sputum, blood plasma and serum, nasopharyngeal and oropharyngeal swabs, stool and urine samples [55]. These specimens exhibit viscosities higher than that of water, which has a viscosity of 1.0 cP [58]. For instance, blood viscosity ranges from approximately 3.5 to 5.5 cP [59], plasma viscosity is around 1.2 to 1.3 cP [59], and saliva viscosity ranges from 1.01 to 1.21 cP [60]. For that reason, MB dye was dispersed in liquid droplets with varying viscosities, both with and without the application of acoustic streaming. The variation of liquid viscosities were manipulated by mixing glycerol with dH_2O at concentrations ranging from 6.25 % to 50 %, corresponding to viscosities (at 25 °C) of 1.08 to 6.86 cP [61]. The results (Fig. 2) show that the average time required for homogeneous mixing of MB dye in glycerol at different concentrations was reduced by approximately 84 % to 88 % when acoustic streaming was applied, compared to mixing without acoustic streaming. This reduction was observed across all tested electrodes which are SPGE, SPCE, and SPCE/Ag (Fig. S1). These findings are consistent with previous study [62] which demonstrated that acoustic streaming reduces the time for fluid mixing. The application of acoustic streaming also has improved the overall analyte micromixing performance and diffusion rate in a sample compared to an incubation system without it [63].

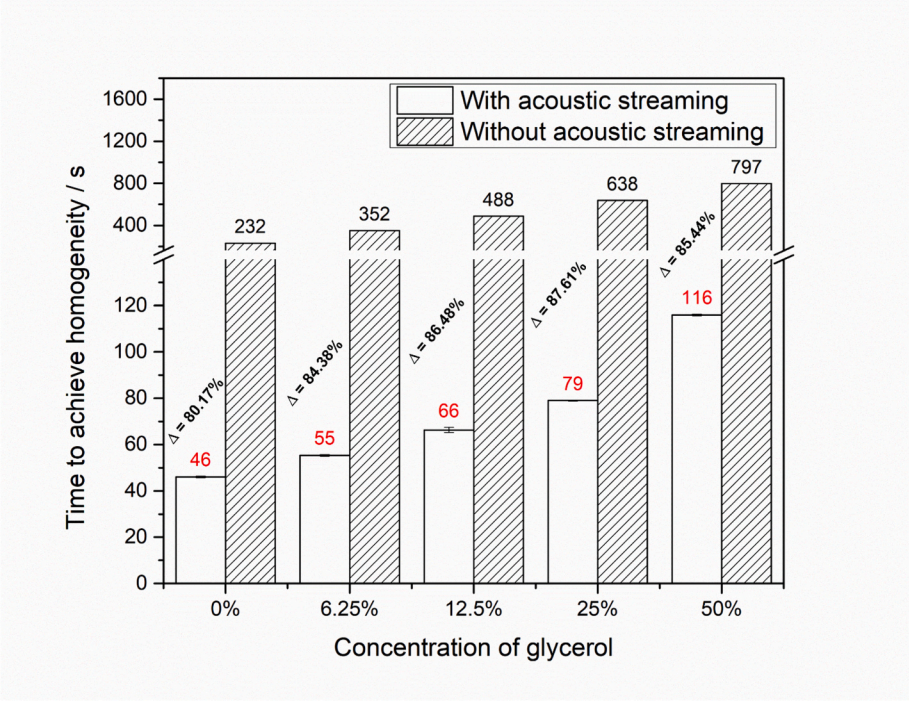

Fig. 2. Average time required for methylene blue (MB) dye to achieve homogenous dispersion in liquid droplets of varying viscosity, with and without acoustic streaming. Viscosity was adjusted by mixing glycerol (6.25–50 %) into dH_2O, while 0 % glycerol comprises of pure dH_2O. Acoustic streaming application has reduced dispersion time across all viscosity levels by approximately 80–88 %, compared to passive incubation. No apparent difference in mixing behavior was observed between electrode platforms (SPGE, SPCE, SPCE/Ag; Fig. S1) due to similar geometry and bulk ceramic composition, therefore, data shown represents the average of all platforms. Error bars indicate the standard deviation ($N = 3$). (For interpretation of the references to colour in this figure legend, the reader is referred to the web version of this article.)

3.2. Evaluation of adsorption by using acoustic streaming through the adsorption of MB dye on cellulose-acetate graphene oxide (CA-GO) beads

After sample mixing capability was evaluated, the impact of acoustic streaming on the adsorption of biomolecules was assessed. Specifically, the adsorption of MB dye onto CA-GO beads was monitored in both the absence and presence of acoustic streaming. The measurement was conducted electrochemically through CV characterization (Fig. S2). The principle behind this study is that MB, being a cationic dye [64], enhances the conductivity of CA-GO beads upon adsorption [65]. In this study, acoustic streaming was applied for varying incubation durations [66] to investigated the impact of enhanced MB adsorption on the CA-GO beads. The difference in MB adsorption, with and without acoustic streaming, was assessed electrochemically by comparing the ΔI_{pa} (Fig. 3(A)) and ΔI_{pc} (Fig. 3(B)). Overall, the conductivity of CA-GO beads following MB adsorption was higher with the application of acoustic streaming compared to adsorption without it. For adsorption with acoustic streaming, the conductivity of the CA-GO beads increased with longer incubation times, reaching a plateau after 8 min, beyond which no apparent improvement was observed up to 16 min. This indicates that 8 min is the optimal duration for MB adsorption under these conditions. In contrast, the conductivity of the CA-GO beads remained low after MB had been adsorbed in the absence of acoustic streaming, even after incubation for 16 min.

In addition to incubation time, the effect of acoustic actuation frequency and amplitude on biomolecule adsorption was also assessed. This study also employed the concept of MB dye adsorption onto CA-GO beads as an adsorption model. The results demonstrated that both the ΔI_{pa} and ΔI_{pc} from the CV analysis (Fig. 4(A)) increased with the increment of actuation frequencies, peaking at 2 MHz (Fig. 4(C)). This trend indicates that higher acoustic streaming frequencies enhanced the adsorption of MB onto the CA-GO beads. However, after the frequency was further increased to 4 MHz, both ΔI_{pa} and ΔI_{pc} decreased, indicating a reduction in conductivity, which indicated a decrement in MB adsorption. These observations were attributed to the resonance of piezoelectric transducer at 2 MHz. In other words, actuating the transducer at its resonance frequency will allow the piezoelectric plate to vibrate at largest amplitude [67], thus delivering optimum acoustic power into solution. This will then create an optimum acoustic streaming inside the solution which increased the adsorption.

Next, the amplitude of acoustic streaming was evaluated by examining the adsorption of MB onto CA-GO beads. CV analysis (Fig. 4(B)) was used to indirectly assess adsorption by measuring the improvement in conductivity following MB adsorption. The results, as indicated by the changes in ΔI_{pa} and ΔI_{pc} (Fig. 4(D)), showed that the conductivity of CA-GO beads increased with the increment of acoustic streaming amplitudes. This improvement can be attributed to the enhancement of fluid flow within the sample, which facilitated better mixing and promoted more effective adsorption of biomolecules as the amplitude increased [68].

3.3. Applicability of acoustic streaming in improving the sensing of NDV through direct detection immunoassay

This part of the study aimed at evaluating the use of acoustic streaming to enhance the detection of NDV through a direct detection immunoassay strategy. The optimized parameters for acoustic streaming, including an 8 min application duration, a frequency of 2 MHz, and an amplitude of 20 V, as determined in Section 3.2, were applied in this study. The amplitude of 20 V was specifically chosen because it produced a stable and consistent acoustic streaming effect that was easily observable to the naked eyes, unlike other tested amplitudes (16 to 19 V), which were less visually discernible [32].

3.3.1. Fabrication of NDV sensing electrode

The NDV sensing platform fabrication started with the optimization of anti-NDV concentration as a bioreceptor on SPGE/CEGU/EDC:NHS. Based on the results (Fig. S3), the optimal concentration of anti-NDV was determined to be 40 ng μL^{-1}. The DPV characterizations confirmed the immobilization of anti-NDV on SPGE/CEGU/EDC:NHS (Fig. 5(A)). The formation of the CEGU SAM on the SPGE working electrode resulted in an I_{pa} reduction of 35.97 ± 2.76 %, attributed to the carboxylic groups of CEGU, which hindered electron transfer at the electrode-electrolyte interface [69]. Additionally, a shift in the oxidation potential peak of the $Fe(CN)_6^{4-}$ anion was observed, moving from 0.115 V (bare SPGE) to −0.025 V (SPGE/CEGU). This shift was associated with improved oxidation of $Fe(CN)_6^{4-}$ due to the presence of oxidative species contributed by the carboxyl-end groups of CEGU. Consequently, the $Fe(CN)_6^{4-}$ oxidation occurred earlier during the DPV potential sweep on SPGE/CEGU (−0.025 V) compared to the bare SPGE (0.115 V) [70,71]. The coupling reaction of EDC:NHS that activated the carboxyl end of CEGU (SPGE/CEGU/EDC:NHS) caused the I_{pa} to increase by 112.53 ± 6.47 %. This increment of I_{pa} was attributed to the reduction of carboxyl groups, which reduced the electrostatic repulsion between the carboxyl groups and the $[Fe(CN)_6]^{3-/4-}$ anion, thereby enhancing electron transfer at the electrode-electrolyte interface [72]. Anti-NDV

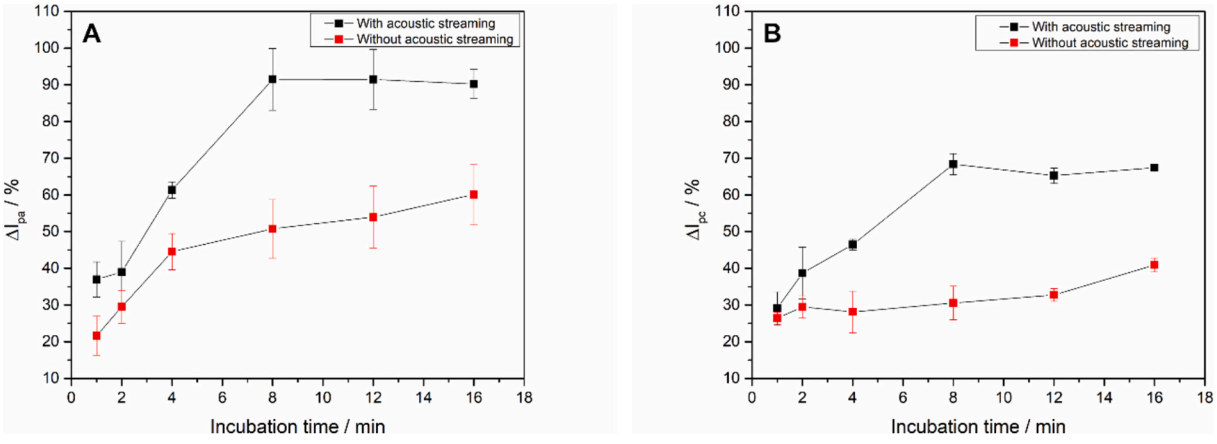

Fig. 3. CV response upon MB adsorption onto CA-GO beads on SPCE at different incubation times. (A) ΔI_{pa} of CV response after MB adsorption on CA-GO beads. (B) ΔI_{pc} of CV response after MB adsorption on CA-GO beads. Adsorption of MB improved the conductivity of the CA-GO beads. For incubation with acoustic streaming, current responses increased as the increment of incubation time went from 1 to 8 min, with no apparent increment can be seen up to 16 min. For incubation without acoustic streaming, the current response steadily increased from 1 min to 16 min of incubation duration. The current response for the incubation with acoustic streaming was significantly higher than incubation without acoustic streaming actuation. Error bars indicate the standard deviation ($N = 3$).

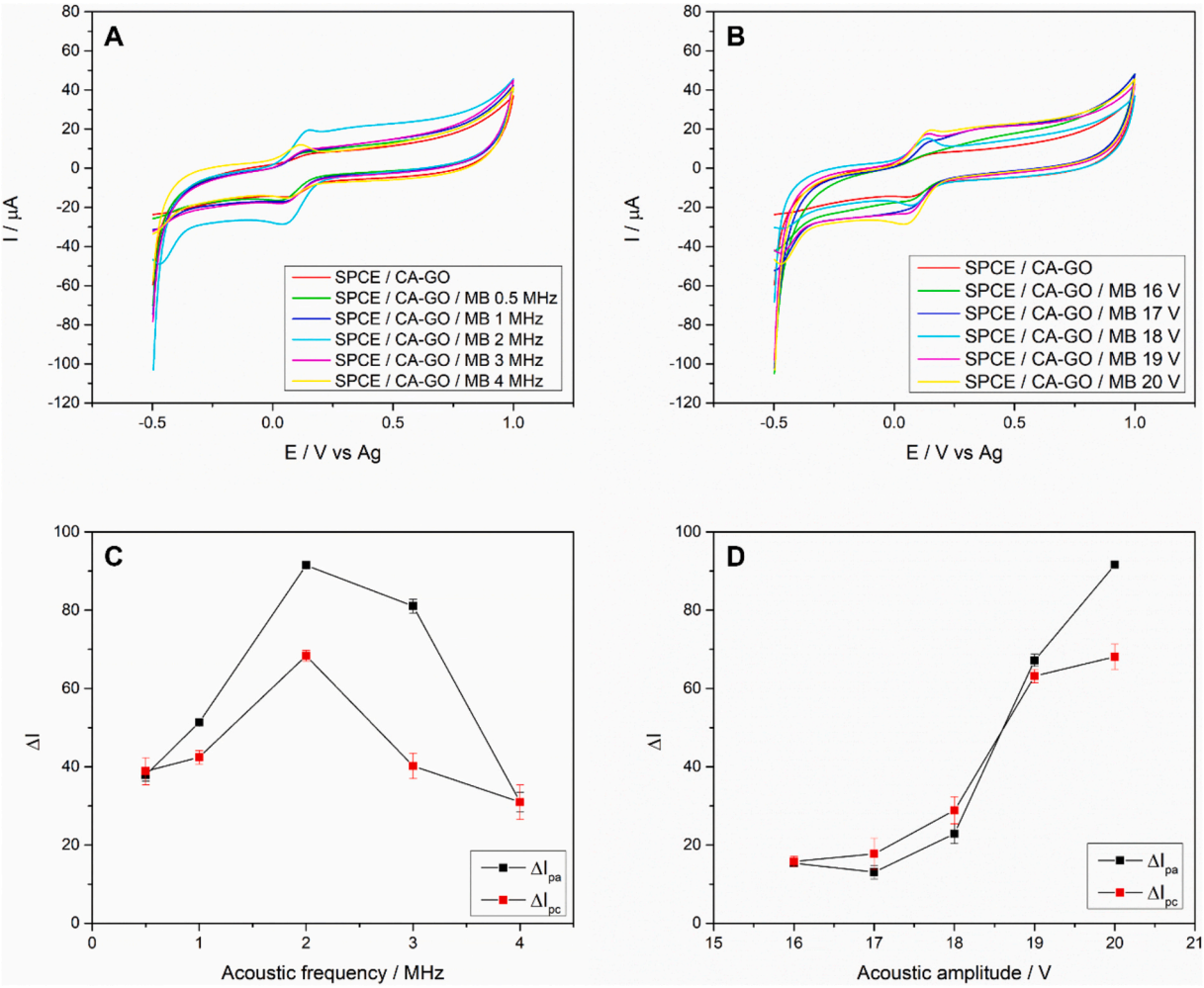

Fig. 4. CV response upon MB adsorption onto CA-GO beads under different acoustic streaming conditions. A) CV characterization of CA-GO/MB incubation at different actuation frequencies ranging from 0.5 to 4 MHz. (B) CV characterization of CA-GO/MB incubation at different actuation amplitudes ranging from 16 to 20 V. (C) ΔI of MB adsorption onto CA-GO beads at different acoustic actuation frequency. From the CV current responses, MB adsorption was optimally seen at the actuated frequency of 2 MHz. (D) ΔI of MB adsorption onto CA-GO beads at different acoustic actuation amplitude with a constant frequency of 2 MHz. From the CV current responses, MB adsorption was increased from supplied amplitude of 16 to 20 V. Error bars indicate the standard deviation ($N = 3$).

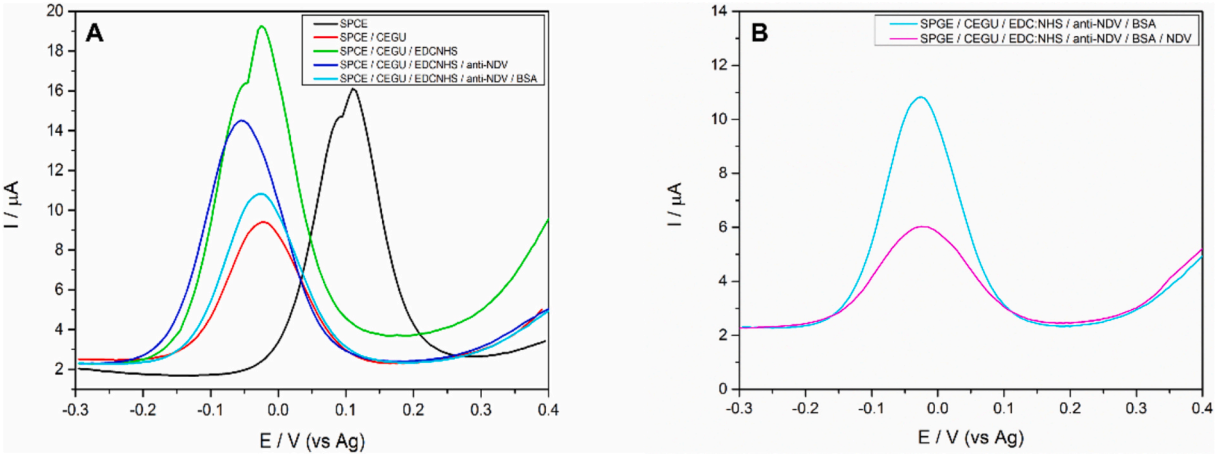

Fig. 5. Electrochemical analysis of anti-NDV immobilization on SAM-modified electrode through DPV. (A) DPV characterization in 5 mM $K_3Fe(CN)_6$ and $K_4Fe(CN)_6$ as redox probe and 0.1 M KCl as supporting electrolyte. Bare SPGE (black line), SPGE/CEGU (red line), SPGE/CEGU/EDC:NHS (green line), SPGE/CEGU/EDC:NHS/anti-NDV (blue line), SPGE/CEGU/EDC:NHS/anti-NDV/BSA (cyan line). (B) Reduction of I_{pa} in DPV characterization after the incubation of 20 HA μL^{-1} NDV on SPGE/CEGU/EDC:NHS/anti-NDV/BSA showing the functionality of the sensing platform in detecting the target analyte. (For interpretation of the references to colour in this figure legend, the reader is referred to the web version of this article.)

immobilization on SPGE/CEGU/EDC:NHS has produced a reduction in I_{pa} by 12.63 ± 1.80 %. The blocking of free and empty spaces by BSA caused the I_{pa} to reduce for 29.77 ± 7.88 %. Reduction of I_{pa} by both anti-NDV and BSA were due to the non-conductive nature of proteins, which hindered the electron transfer at the electrode-electrolyte surface [72,73]. After a complete anti-NDV sensing platform (SPGE/CEGU/EDC:NHS/anti-NDV/BSA) was assembled, an evaluation for NDV detection was performed. This was done by incubating NDV in PBS (20 HA μL^{-1}) for 20 min at room temperature. DPV analysis revealed a further reduction in I_{pa} (Fig. 5(B)), indicating the formation of an immunocomplex between immobilized anti-NDV and NDV on the electrode surface [74].

3.3.2. Sensitivity study of NDV sensing platform

Following the fabrication of SPGE/CEGU/EDC:NHS/anti-NDV/BSA as the sensing platform, NDV spiked in PBS (0.156 to 20 HA μL^{-1}) was incubated to determine the limit of detection (LoD). The NDV incubation was performed under two conditions, with and without acoustic streaming. For incubation with acoustic streaming, optimized parameters (20 V amplitude, 2 MHz frequency, and 8 min sample incubation duration) were applied. In contrast, incubation without acoustic streaming was conducted for 20 min, similar to the incubation conditions done in a previously published study [47]. A negative control (avidin in PBS, 500 ng μL^{-1}, 10 µL) was incubated on SPGE/CEGU/EDC:NHS/anti-NDV/BSA prior to NDV detection at different concentrations for LoD determination. This test was done to ensure all free and empty spaces for binding on the electrode were blocked by BSA. The result (Fig. S4) showed that there was no apparent ΔI_{pa} (0.70 ± 1.08 %) following avidin incubation on the fabricated electrode, indicating adequate BSA blocking.

Following that, NDV at different concentrations were incubated on separate SPGE/CEGU/EDC:NHS/anti-NDV/BSA. DPV characterization after immunocomplex formation revealed the decrement in I_{pa} as the NDV concentration increased from 0.156 to 20 HA μL^{-1} for both incubation with (Fig. 6(A)) and without (Fig. 6(B)) acoustic streaming. This was due to the non-conductive properties of proteins including viruses, which hindered the electron transfer at the electrode-electrolyte interface [72]. From the plot of ΔI_{pa} versus [NDV] for NDV detection without acoustic streaming, fitted with the Langmuir model (Eq. 4, Fig. 6(C)), the $\Delta I_{pa\ max}$ was calculated as 54.38 ± 0.79 %, while the K_L between anti-NDV and NDV at different concentrations was determined to be 0.45 ± 0.05 µL HA^{-1} (R^2 = 0.99), indicating a good binding affinity.

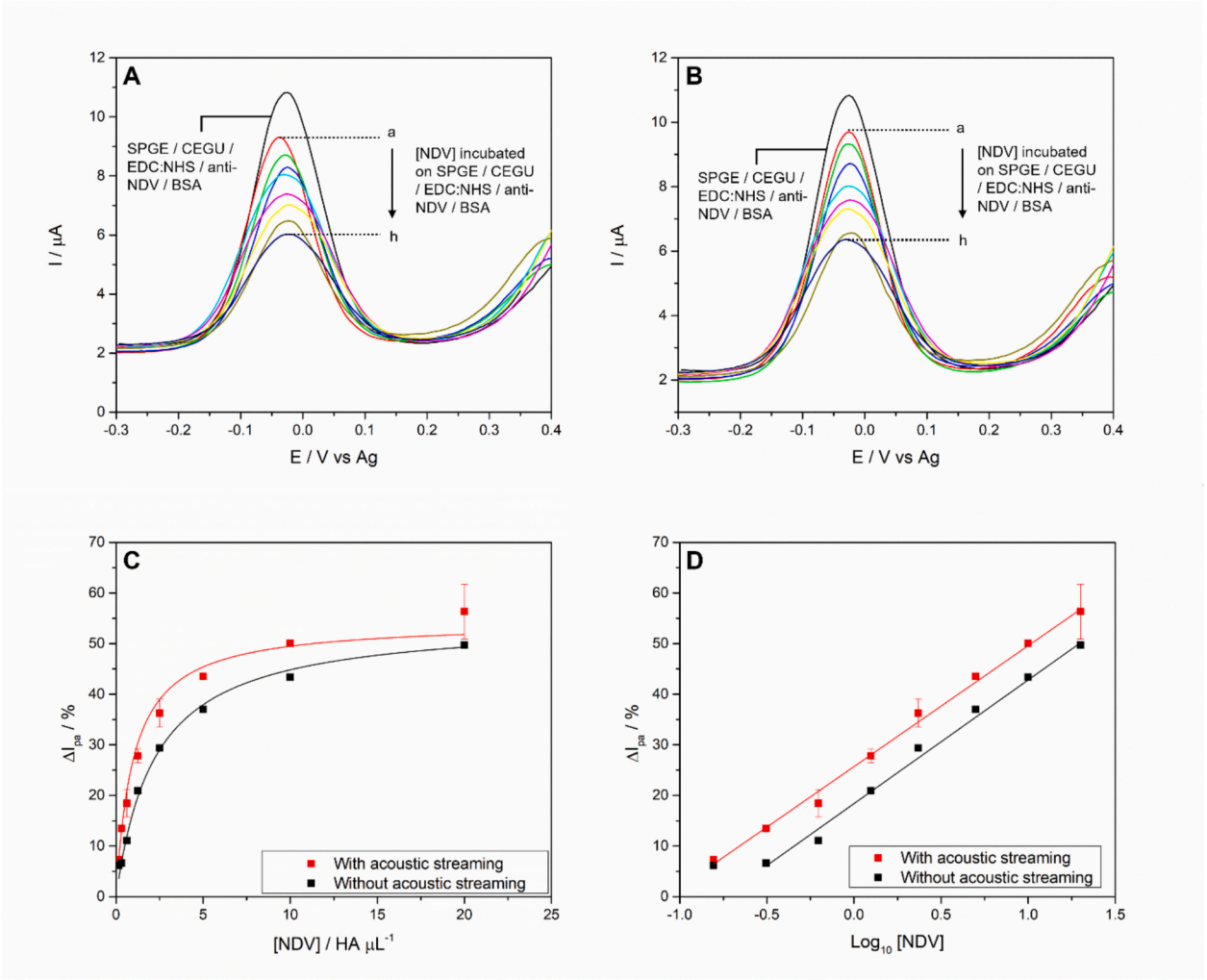

Fig. 6. Sensitivity of NDV detection in PBS through a direct detection immunoassay with SAM chemistry. (A) DPV characterization for NDV detection at different concentrations with acoustic streaming application. (B) DPV characterization for NDV detection at different concentrations without acoustic streaming application. [NDV] = (a) 0.156 HA μL^{-1}, (b) 0.313 HA μL^{-1}, (c) 0.625 HA μL^{-1}, (d) 1.25 HA μL^{-1}, (e) 2.5 HA μL^{-1}, (f) 5 HA μL^{-1}, (g) 10 HA μL^{-1}, and (h) 20 HA μL^{-1}. (C) Binding isotherm for anti-NDV at different concentrations of NDV in PBS based on the Langmuir model. (D) Linear relationship plot between ΔI_{pa} and $\log_{10}$ concentration of NDV for detection with acoustic streaming ($\Delta I_{pa} = 24.101 \log_{10}$ [NDV] + 25.704, $R^2 = 0.99$) and without acoustic streaming ($\Delta I_{pa} = 24.9 \log_{10}$ [NDV] + 18.389, R^2 = 0.99). Error bars indicate the standard deviation ($N = 3$).

However, $\Delta I_{pa\ max}$ and K_L for NDV incubation with the application of acoustic streaming was determined to be at 54.76 ± 1.47 % and 1.01 ± 0.06 μL HA^{-1} ($R^2 = 0.99$), respectively. From these results, it was found that acoustic streaming improved K_L by 124.4 % while having similar $\Delta I_{pa\ max}$ value, despite the sample incubation time being reduced by 60 % compared to 20 min incubation without acoustic streaming. The LoD (at 3σ m^{-1}) was then determined from plotted linear relationship (Fig. 6 (D), where NDV incubation without acoustic streaming produced a LoD of 1.57 HA μL^{-1}, while the same incubation with acoustic streaming produced a 7 % lower LoD (1.46 HA μL^{-1}). The observed improvement especially in K_L value, along with nearly the same $\Delta I_{pa\ max}$ and LoD, despite the shorter incubation duration in NDV detection with acoustic streaming. Shortening the assay duration while achieving nearly similar or better LoD is highly desirable in any biosensing application, as it enables faster throughput and more rapid diagnosis of diseases or infections [75,76]. These findings are consistent with previous study [77] which demonstrated that the incorporation of acoustic streaming improves the overall electrochemical sensing performance.

A comparative analysis between the present sensing platform and previously reported NDV and other target analytes detection is presented in Table 1. As shown in the table, previous studies [78,79] have demonstrated improved LoD through the incorporation of acoustic streaming, provided that the incubation duration was maintained for both conditions of with and without acoustic streaming. In contrast to their findings, the voltammetric NDV detection strategy in this study shows that a comparable LoD can be achieved in both incubation conditions. However, the incorporation of acoustic streaming has shortened the assay duration. This observation is consistent with findings reported by Zhang et al. [80] where acoustic streaming application has been demonstrated to be able in reducing the antigen-antibody incubation duration in conventional ELISA performed in 96-well microplates. While other biosensor studies [81–84] typically require at least 60 min for target analyte incubation, and a recent study by Lee et al. [85] indicated that a minimum of 20 min is required to ensure sufficient interaction between the target analyte and the bioreceptor, the present voltammetric detection approach demonstrates that the incubation time can be reduced to only 8 min through the incorporation of acoustic streaming.

3.3.3. Specificity and selectivity studies of NDV sensing platform

The specificity of the fabricated NDV sensing platform was evaluated by incubation of 1:1000 diluted allantoic fluid from embryonated chicken eggs on the fabricated sensing platform. The proteins contained in the allantoic fluid such as fibronectin, ovotransferrin, alpha-fetoprotein, serum albumin, and ovalbumin [86] acted as the interferences in this specificity study.

The I_{pa} of DPV showed a reduction after the fabricated sensing platform had been incubated with 1:1000 diluted allantoic fluid (Fig. 7 (A)), NDV in PBS (Fig. 7(B)) and NDV in 1:1000 diluted allantoic fluid (Fig. 7(C)), respectively. However, the incubation of 1:1000 diluted allantoic fluid on the sensing platform produced ΔI_{pa} values of only 2.73 % and 5.69 % for incubation with and without acoustic streaming, respectively (Fig. 7(D)). Considering the calculated LoDs for NDV detection, which corresponded to ΔI_{pa} values of approximately 29.63 % and 23.23 % (based on the linear equations in Fig. 6), and the lowest tested NDV concentration (0.156 HA μL^{-1}), which yielded ΔI_{pa} values of 7.32 % and 6.18 % for incubation with and without acoustic streaming respectively, the lower ΔI_{pa} values observed during allantoic fluid incubation confirmed the specificity of the fabricated sensing platform. This indicates that the platform is selective only for NDV and not reactive to proteins in the allantoic fluid, i.e. no apparent cross-reactivity has been observed in allantoic fluid. Furthermore, the incorporation of acoustic streaming reduced the ΔI_{pa} caused by allantoic fluid by approximately 3 % compared to incubation without acoustic streaming. This reduction can be attributed to the anti-biofouling effect of acoustic streaming. The latter enhanced microconvection within the fluid, which resulted in the increment of fluid movement causing the removal of low-affinity non-specific biomolecules, thereby promoting more specific binding interactions of immobilized anti-NDV with NDV [39]. In

Table 1
Sensing strategies and performance of other published biosensors and immunoassays.

Detection method	Bioreceptor	Target analyte	Linear range	LoD	Assay duration (min)*	Acoustic streaming incorporation	Reference
Biosensor (CV voltammetric electrochemical immunosensor)	Anti-NDV IgY	NDV	10^2 to 10^6 EID_{50} mL^{-1}	5 EID_{50} mL^{-1}	60	No	[81]
Biosensor (DPV voltammetric electrochemical immunosensor)	Chitosan-AuNPs-conjugated monolclonal anti-NDV and copper-chitosan-graphene-conjugated polyclonal anti-NDV	NDV	$10^{0.13}$ to $10^{5.13}$ EID_{50} in 0.1 mL	$10^{2.09}$ EID_{50} in 0.1 mL	70	No	[83]
Immunoassay (ELISA)	Ferritin-fused nanobody and nanobody-fused reporter	NDV	2^0 to 2^8 HA	2^2 HA	110	No	[82]
Immunoassay (ELISA)	Anti-protein A antibody	HRP-conjugated goat anti-chicken antibody	n.a.	n.a.	60	No	[80]
Immunoassay (ELISA)	Anti-protein A antibody	HRP-conjugated goat anti-chicken antibody	n.a.	n.a.	15	Yes	[80]
Biosensor (fluorescent-based microfluidic aptasensor)	Aptamer sequences targeting thrombin	Thrombin	0.1 to 200 nM	139 pM	45	No	[78]
Biosensor (fluorescent-based microfluidic aptasensor)	Aptamer sequences targeting thrombin	Thrombin	0.1 to 200 nM	15 pM	45	Yes	[78]
Biosensor (chronoamperometric electrochemical biosensor)	Nanozyme	Dopamine	0.5 to 100 μM	0.382 μM	6.7	No	[79]
Biosensor (chronoamperometric electrochemical biosensor)	Nanozyme	Dopamine	0.2 to 100 μM	0.084 μM	6.7	Yes	[79]
Biosensor (DPV voltammetric electrochemical immunosensor)	Anti-NDV	NDV	0.313 to 20 HA μL^{-1}	1.57 HA μL^{-1}	20	No	This study
Biosensor (DPV voltammetric electrochemical immunosensor)	Anti-NDV	NDV	0.156 to 20 HA μL^{-1}	1.46 HA μL^{-1}	8	Yes	This study

n.a. = not applicable as the study did not incorporate the linear range of detection and calculate the LoD.

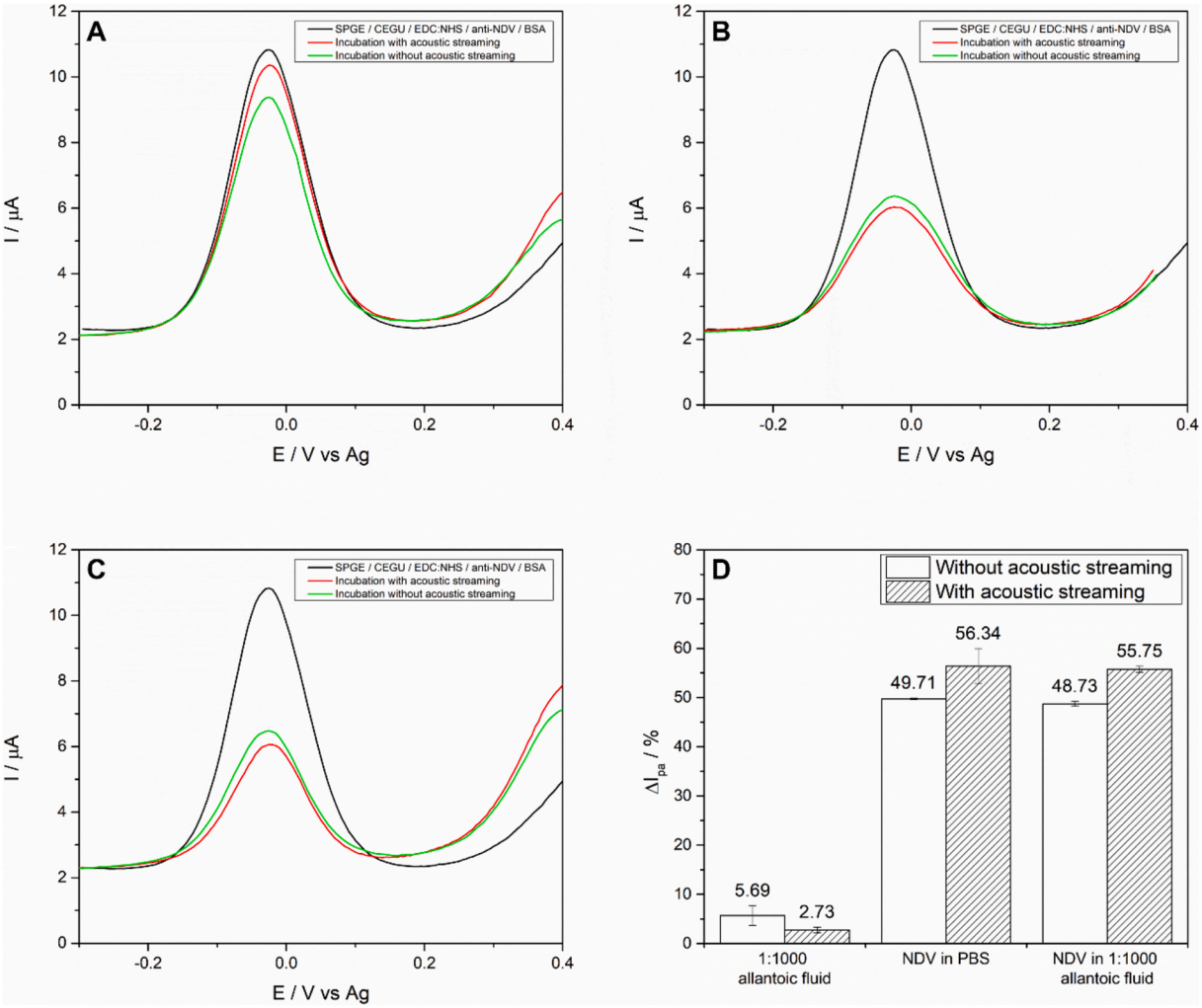

Fig. 7. Selectivity and specificity study of NDV sensing platform utilizing the modified SPGE/CEGU/EDC:NHS/anti-NDV/BSA electrode. (A) DPV characterization for the incubation of 1:1000 diluted allantoic fluid on SPGE/CEGU/EDC:NHS/anti-NDV/BSA with and without acoustic streaming application. (B) DPV characterization for the incubation of NDV in PBS on SPGE/CEGU/EDC:NHS/anti-NDV/BSA with and without acoustic streaming application. (C) DPV characterization for the incubation of NDV in 1:1000 diluted allantoic fluid on SPGE/CEGU/EDC:NHS/anti-NDV/BSA with and without acoustic streaming application. (D) ΔI_{pa} for each sample incubation with and without acoustic streaming on fabricated SPGE/CEGU/EDC:NHS/anti-NDV/BSA. Error bars indicate the standard deviation ($N = 3$).

reference to the recent published study by Abd Muain et al. [47], which highlighted a reduction in non-specific binding through the application of polyethylene glycol-containing alkanethiol in their sensing platform assembly, the present NDV detection study demonstrates a synergistic effect when combining the same alkanethiol with acoustic streaming. In other words, the integration of acoustic streaming with a hydrophilic layer in the biosensor development has shown an enhanced ability to mitigate non-specific binding problems.

The fabricated sensing platform was incubated with NDV (20 HA μL^{-1}) spiked in 1:1000 diluted allantoic fluid to evaluate its selectivity performance. The incubation was done both with and without the incorporation of acoustic streaming. The results (Fig. 7(D)) demonstrated that the sensing platforms successfully detected the presence of NDV in the sample, with relative standard deviation (RSD) values of 0.72 % and 1.41 %, respectively, when compared to their respective positive control ΔI_{pa}. These findings confirm that both incubation strategies were effective in detecting NDV in 1:1000 diluted allantoic fluid. However, the incorporation of acoustic streaming resulted in a higher ΔI_{pa}, which is consistent with the sensitivity study shown in Fig. 6, indicating more immunocomplexes have formed on the sensing surface compared to incubation without acoustic streaming. This trend was observed for NDV spiked in both PBS and 1:1000 diluted allantoic fluid.

3.3.4. *Detection of NDV in diluted allantoic fluid*

The ability of the NDV sensing platform to detect the target analyte in real samples was done by the incubation of NDV spiked in 1:1000 diluted allantoic fluid. The NDV concentrations were the same as in the sensitivity study (Section 2.6.2), and the incubations were done in the presence and absence of acoustic streaming. As expected, I_{pa} in DPV analyses for both incubation with (Fig. 8(A)) and without (Fig. 8(B)) acoustic streaming have shown a decrement in trend as the NDV concentration incubated on SPGE/CEGU/EDC:NHS/anti-NDV/BSA increased. The Langmuir model (Eq. 4) fitting to the plot of ΔI_{pa} against [NDV] (Fig. 8(C)) for NDV detection without acoustic streaming provided a $\Delta I_{pa\ max}$ to be 54.96 ± 2.14 %, while K_L between anti-NDV and NDV at different concentrations was at 0.40 ± 0.02 µL HA^{-1} (R^2 = 0.98). However, the corresponding data but with the application of acoustic streaming displayed $\Delta I_{pa\ max}$ and K_L values to be at 59.24 ± 1.16 % and 0.65 ± 0.08 µL HA^{-1} (R^2 = 0.99), respectively. These demonstrated that the incorporation of acoustic streaming in the detection of NDV has improved both $\Delta I_{pa\ max}$ and K_L values by approximately 7.8 % and 62.5 %, respectively. Moreover, these also proved the ability of acoustic streaming in enhancing target analyte detection, even in a complex sample matrix like embryonated chicken eggs allantoic fluid. However, the improvements observed with acoustic

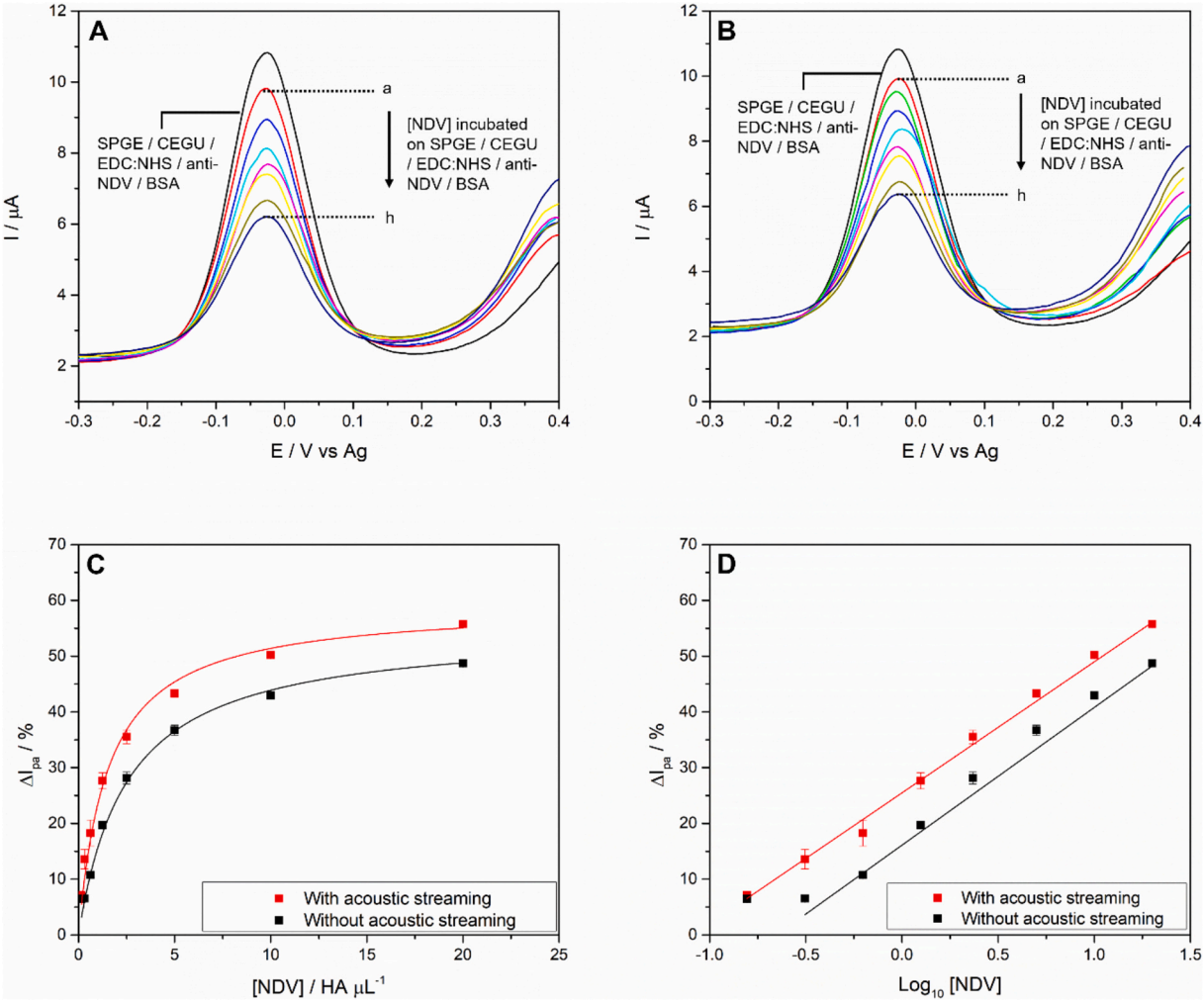

Fig. 8. Detection of NDV in 1:1000 diluted allantoic fluid with and without the application of acoustic streaming. (A) DPV characterization for NDV detection at different concentrations with acoustic streaming application. (B) DPV characterization for NDV detection at different concentrations without acoustic streaming application. [NDV] = (a) 0.156 HA μL^{-1}, (b) 0.313 HA μL^{-1}, (c) 0.625 HA μL^{-1}, (d) 1.25 HA μL^{-1}, (e) 2.5 HA μL^{-1}, (f) 5 HA μL^{-1}, (g) 10 HA μL^{-1}, and (h) 20 HA μL^{-1}. (C) Binding isotherm for anti-NDV at different concentrations of NDV in 1:1000 diluted allantoic fluid based on Langmuir model. (D) Linear relationship plot between ΔI_{pa} and $\log_{10}$ concentration of NDV for detection with acoustic streaming ($\Delta I_{pa} = 23.989 \log_{10}$ [NDV] + 25.491, $R^2 = 0.99$) and without acoustic streaming ($\Delta I_{pa} = 24.693 \log_{10}$ [NDV] + 17.812, $R^2 = 0.99$). RSD values were calculated to be in the range of 0.23 to 2.07 % and 0.56 to 4.31 % for NDV detection with and without acoustic streaming, respectively. Error bars indicate the standard deviation ($N = 3$).

streaming were less pronounced than those achieved in NDV detection in PBS (Section 3.3.2), particularly for the value of K_L. This reduction was likely attributed to interference from non-specific proteins in the allantoic fluid, which could disrupt the formation of immunocomplexes between immobilized anti-NDV and NDV on the electrode. The LoDs (at 3σ m^{-1}) were then determined from the fitted linear relationship between ΔI_{pa} against $\log_{10}$ [NDV] (Fig. 8(D)). NDV detection with acoustic streaming produced an LoD of 1.45 HA μL^{-1}, compared to the detection without acoustic streaming which resulted in an LoD of 1.62 HA μL^{-1}. These LoD values were equivalent to those reported in Section 3.3.2, where the incorporation of acoustic streaming produced a lower LoD compared to detection approach without it.

The reproducibility [87], as well as precision and accuracy [73] of ΔI_{pa} measurements for NDV detection in diluted allantoic fluid were also evaluated through the RSD values determination (Table 2) for each incubated NDV concentration, based on results obtained in Section 3.3.2.

These findings highlight the ability of both detection strategies, whether with the incorporation of acoustic streaming or not, to reliably detect NDV spiked in diluted allantoic fluid. However, the incorporation of acoustic streaming in the detection strategy has enhanced the detection performance in terms of the ability to achieve a lower LoD while having shorter period of sample incubation.

Table 2
RSD value for each NDV concentration incubated with and without the application of acoustic streaming.

[NDV] / HA μL^{-1}	RSD / %	
	With acoustic streaming	Without acoustic streaming
0.156	2.07	3.4
0.313	0.43	1.22
0.625	0.68	2.32
1.25	0.54	4.31
2.5	1.53	3.02
5	0.35	0.56
10	0.23	0.67
20	0.72	1.42

4. Conclusion

Acoustic streaming has been incorporated into a biosensing system

by placing a piezoelectric plate beneath a SPGE to generate mechanical forces that enhance convective transport in incubated samples. The ultrasonic vibrations initiated fluid flow in the incubated samples which improved both fluid micromixing and adsorption of biomolecules. Micromixing efficiency was assessed by dispersing MB dye in liquid droplets at varying concentrations on different electrode surfaces. Acoustic streaming reduced the time required for homogeneous dispersion of MB in the liquid droplets by approximately 80 to 88 %, regardless of the electrode surface type. From the adsorption analysis by using MB dye solution and CA-GO beads, it was found that the incorporation of acoustic streaming in the adsorption process shortened the duration (8 min) needed to achieve maximum adsorption of MB by CA-GO beads compared to the same adsorption without acoustic streaming application, while the optimum applied frequency and amplitude for acoustic actuation was found to be at 2 MHz and 20 V, respectively. An electrochemical immunosensor was then developed for NDV detection, utilizing anti-NDV immobilized on PEG-containing alkanethiol-modified SPGE as bioreceptor. The detection system with acoustic streaming achieved a lower LoD, despite a shorter incubation time of 8 min compared to 20 min for the detection system without acoustic streaming. This improvement was due to the microconvection facilitated by acoustic streaming, which enhanced the interaction between the NDV and the anti-NDV on the sensing platform. Additionally, the integration of acoustic streaming reduced non-specific binding of proteins on the sensing platform, thus enhancing the detection selectivity. This could also be due to microconvection providing a fluid flow which may have constantly removed the non-specific biomolecules from being adsorbed onto the sensing surface. Based on the results shown in this study, the incorporation of acoustic streaming in biosensor development offers a promising approach in achieving comparable LoD and improving selectivity and specificity, while reducing the total assay duration.

CRediT authorship contribution statement

Mohamad Farid Abd Muain: Writing – review & editing, Writing – original draft, Visualization, Validation, Project administration, Methodology, Investigation, Formal analysis, Data curation, Conceptualization. **Amir Syahir Amir Hamzah:** Writing – review & editing, Validation, Supervision, Project administration, Methodology, Conceptualization. **Suet Lin Chia:** Writing – review & editing, Validation, Supervision, Resources, Methodology, Funding acquisition, Conceptualization. **Khatijah Yusoff:** Writing – review & editing, Validation, Supervision, Resources, Methodology, Funding acquisition, Conceptualization. **Hong Ngee Lim:** Writing – review & editing, Validation, Supervision, Resources, Methodology, Conceptualization. **Shinya Ikeno:** Writing – review & editing, Supervision, Resources, Methodology, Funding acquisition, Conceptualization. **Thomas Laurell:** Writing – review & editing, Validation, Supervision, Resources, Methodology, Conceptualization. **Asilah Ahmad Tajudin:** Writing – review & editing, Validation, Supervision, Resources, Project administration, Methodology, Funding acquisition, Conceptualization.

Declaration of competing interest

The authors declare that they have no known competing financial interests or personal relationships that could have appeared to influence the work reported in this paper.

Acknowledgements

This project is supported by the Ministry of Science, Technology, and Innovation (MOSTI), Malaysia under the Dana Pembangunan dan Pengukuhan Penghasilan Vaksin Negara (DPVN) funding. The student expenses were supported by the Excellence Student Program from Public Service Department, Malaysia, and Japan Student Services Organization (JASSO), Japan.

Appendix A. Supplementary data

Supplementary data to this article can be found online at https://doi.org/10.1016/j.bioelechem.2025.109043.

Data availability

No data was used for the research described in the article.

References

[1] X. Yang, C. Gong, Y. Wang, Y. Luo, Y.-J. Rao, G.-D. Peng, Y. Gong, A sequentially bioconjugated optofluidic laser for wash-out-free and rapid biomolecular detection, Lab Chip 21 (2021) 1686–1693, https://doi.org/10.1039/D0LC01332C.
[2] R. Ahirwar, A. Bhattacharya, S. Kumar, Unveiling the underpinnings of various non-conventional ELISA variants: a review article, expert rev, Mol. Diagn. 22 (2022) 761–774, https://doi.org/10.1080/14737159.2022.2117615.
[3] M. Park, J. Won, B.Y. Choi, C.J. Lee, Optimization of primer sets and detection protocols for SARS-CoV-2 of coronavirus disease 2019 (COVID-19) using PCR and real-time PCR, Exp. Mol. Med. 52 (2020) 963–977, https://doi.org/10.1038/s12276-020-0452-7.
[4] M.A. MacMullan, A. Ibrayeva, K. Trettner, L. Deming, S. Das, F. Tran, J.R. Moreno, J.G. Casian, P. Chellamuthu, J. Kraft, K. Kozak, F.E. Turner, V.I. Slepnev, L.M. Le Page, ELISA detection of SARS-CoV-2 antibodies in saliva, Sci. Rep. 10 (2020) 20818, https://doi.org/10.1038/s41598-020-77555-4.
[5] S. Edouard, P. Colson, C. Melenotte, F. Di Pinto, L. Thomas, B. La Scola, M. Million, H. Tissot-Dupont, P. Gautret, A. Stein, P. Brouqui, P. Parola, J.-C. Lagier, D. Raoult, M. Drancourt, Evaluating the serological status of COVID-19 patients using an indirect immunofluorescent assay, France, Eur. J. Clin. Microbiol. Infect. Dis. 40 (2021) 361–371, https://doi.org/10.1007/s10096-020-04104-2.
[6] M.P. Kabiraz, P.R. Majumdar, M.M.C. Mahmud, S. Bhowmik, A. Ali, Conventional and advanced detection techniques of foodborne pathogens: a comprehensive review, Heliyon 9 (2023) e15482, https://doi.org/10.1016/j.heliyon.2023.e15482.
[7] R. Calmo, A. Chiadò, S. Fiorilli, C. Ricciardi, Advanced ELISA-like biosensing based on Ultralarge-pore silica microbeads, ACS Appl. Bio Mater. 3 (2020) 5787–5795, https://doi.org/10.1021/acsabm.0c00533.
[8] M.Z.H. Khan, M.R. Hasan, S.I. Hossain, M.S. Ahommed, M. Daizy, Ultrasensitive detection of pathogenic viruses with electrochemical biosensor: state of the art, Biosens. Bioelectron. 166 (2020) 112431, https://doi.org/10.1016/j.bios.2020.112431.
[9] C. Wang, M. Liu, Z. Wang, S. Li, Y. Deng, N. He, Point-of-care diagnostics for infectious diseases: from methods to devices, Nano Today 37 (2021) 101092, https://doi.org/10.1016/j.nantod.2021.101092.
[10] S. Vashist, Point-of-care diagnostics: recent advances and trends, Biosensors 7 (2017) 62, https://doi.org/10.3390/bios7040062.
[11] N.F.D. Silva, M.M.P.S. Neves, J.M.C.S. Magalhães, C. Freire, C. Delerue-Matos, Electrochemical immunosensor towards invasion-associated protein p60: an alternative strategy for listeria monocytogenes screening in food, Talanta 216 (2020) 120976, https://doi.org/10.1016/j.talanta.2020.120976.
[12] E. Vargas, H. Teymourian, F. Tehrani, E. Eksin, E. Sánchez-Tirado, P. Warren, A. Erdem, E. Dassau, J. Wang, Enzymatic/immunoassay dual-biomarker sensing Chip: towards decentralized insulin/glucose detection, Angew. Chem. Int. Ed. 58 (2019) 6376–6379, https://doi.org/10.1002/anie.201902664.
[13] Y. Gao, P. Tran, K. Petkovic-Duran, T. Swallow, Y. Zhu, Acoustic micromixing increases antibody-antigen binding in immunoassays, Biomed. Microdevices 17 (2015) 79, https://doi.org/10.1007/s10544-015-9987-0.
[14] S. Razavi Bazaz, A. Sayyah, A.H. Hazeri, R. Salomon, A. Abouei Mehrizi, M. Ebrahimi Warkiani, Micromixer research trend of active and passive designs, Chem. Eng. Sci. 293 (2024) 120028, https://doi.org/10.1016/j.ces.2024.120028.
[15] C.-Y. Lee, W.-T. Wang, C.-C. Liu, L.-M. Fu, Passive mixers in microfluidic systems: a review, Chem. Eng. J. 288 (2016) 146–160, https://doi.org/10.1016/j.cej.2015.10.122.
[16] N. Toufik Tayeb, K. Amar, K. Sofiane, L. Lakhdar, L. Yahia, Thermal mixing performances of shear-thinning non-Newtonian fluids inside two-layer crossing channels micromixer using entropy generation method: comparative study, Chem. Eng. Process. Process Intensif. 156 (2020) 108096, https://doi.org/10.1016/j.cep.2020.108096.
[17] S. Najjaran, S. Rashidi, M.S. Valipour, A new design of induced-charge electrokinetic micromixer with corrugated walls and conductive plate installation, Int. Commun. Heat Mass Transf. 114 (2020) 104564, https://doi.org/10.1016/j.icheatmasstransfer.2020.104564.
[18] F. Zhang, S. Marre, A. Erriguible, Mixing intensification under turbulent conditions in a high pressure microreactor, Chem. Eng. J. 382 (2020) 122859, https://doi.org/10.1016/j.cej.2019.122859.
[19] J. Wang, Q. Feng, J. Yao, K. Zhao, Insights into a T-type micromixer with novel electromagnetic mixing, Int. J. Heat Mass Transf. 214 (2023) 124468, https://doi.org/10.1016/j.ijheatmasstransfer.2023.124468.
[20] V.R. Faradonbeh, S. Rabiei, H. Rabiei, M. Goodarzi, M.R. Safaei, C.-X. Lin, Power-law fluid micromixing enhancement using surface acoustic waves, J. Mol. Liq. 347 (2022) 117978, https://doi.org/10.1016/j.molliq.2021.117978.

[21] X. Wang, Z. Liu, B. Wang, Y. Cai, Q. Song, An overview on state-of-art of micromixer designs, characteristics and applications, Anal. Chim. Acta 1279 (2023) 341685, https://doi.org/10.1016/j.aca.2023.341685.
[22] W. Wei, Y. Wang, Z. Wang, X. Duan, Microscale acoustic streaming for biomedical and bioanalytical applications, TrAC Trends Anal. Chem. 160 (2023) 116958, https://doi.org/10.1016/j.trac.2023.116958.
[23] B. Cha, S.H. Lee, S.A. Iqrar, H.-G. Yi, J. Kim, J. Park, Rapid acoustofluidic mixing by ultrasonic surface acoustic wave-induced acoustic streaming flow, Ultrason. Sonochem. 99 (2023) 106575, https://doi.org/10.1016/j.ultsonch.2023.106575.
[24] H. Bachman, C. Chen, J. Rufo, S. Zhao, S. Yang, Z. Tian, N. Nama, P.-H. Huang, T. J. Huang, An acoustofluidic device for efficient mixing over a wide range of flow rates, Lab Chip 20 (2020) 1238–1248, https://doi.org/10.1039/C9LC01171D.
[25] A.G. Guex, N. Di Marzio, D. Eglin, M. Alini, T. Serra, The waves that make the pattern: a review on acoustic manipulation in biomedical research, Mater. Today Bio. 10 (2021) 100110, https://doi.org/10.1016/j.mtbio.2021.100110.
[26] N. Hao, Z. Pei, P. Liu, H. Bachman, T.D. Naquin, P. Zhang, J. Zhang, L. Shen, S. Yang, K. Yang, S. Zhao, T.J. Huang, Acoustofluidics-assisted fluorescence-SERS bimodal biosensors, Small 16 (2020), https://doi.org/10.1002/smll.202005179.
[27] M. Afzal, J. Park, J.S. Jeon, M. Akmal, T.-S. Yoon, H.J. Sung, Acoustofluidic separation of proteins using aptamer-functionalized microparticles, Anal. Chem. 93 (2021) 8309–8317, https://doi.org/10.1021/acs.analchem.1c01198.
[28] A.A. Nawaz, D. Soteriou, C.K. Xu, R. Goswami, M. Herbig, J. Guck, S. Girardo, Image-based cell sorting using focused travelling surface acoustic waves, Lab Chip 23 (2023) 372–387, https://doi.org/10.1039/D2LC00636G.
[29] J. Durrer, P. Agrawal, A. Ozgul, S.C.F. Neuhauss, N. Nama, D. Ahmed, A robot-assisted acoustofluidic end effector, Nat. Commun. 13 (2022) 6370, https://doi.org/10.1038/s41467-022-34167-y.
[30] X. Chen, Y. Ning, S. Pan, B. Liu, Y. Chang, W. Pang, X. Duan, Mixing during trapping enabled a continuous-flow microfluidic smartphone immunoassay using acoustic streaming, ACS Sensors. 6 (2021) 2386–2394, https://doi.org/10.1021/acssensors.1c00602.
[31] Y. Li, Y. Zhao, Y. Yang, W. Zhang, Y. Zhang, S. Sun, L. Zhang, M. Li, H. Gao, C. Huang, Acoustofluidics-enhanced biosensing with simultaneously high sensitivity and speed, Microsyst. Nanoeng. 10 (2024) 92, https://doi.org/10.1038/s41378-024-00731-3.
[32] N. Syamila, A.S.A. Hamzah, T. Laurell, Y. Sulaiman, S. Ikeno, W. Siang Tan, A. Ahmad Tajudin, Displacement of PAMAM-au via acoustic streaming on an electrochemical immunosensing platform, J. Micromech. Microeng. 34 (2024) 015001, https://doi.org/10.1088/1361-6439/ad0e42.
[33] N. Garg, D. Boyle, A. Randall, A. Teng, J. Pablo, X. Liang, D. Camerini, A.P. Lee, Rapid immunodiagnostics of multiple viral infections in an acoustic microstreaming device with serum and saliva samples, Lab Chip 19 (2019) 1524–1533, https://doi.org/10.1039/C8LC01303A.
[34] L. Zhang, Z. Tian, H. Bachman, P. Zhang, T.J. Huang, A cell-phone-based Acoustofluidic platform for quantitative point-of-care testing, ACS Nano 14 (2020) 3159–3169, https://doi.org/10.1021/acsnano.9b08349.
[35] Y. Guan, F. Xu, B. Sun, X. Meng, Y. Liu, M. Bai, A hybrid electrically-and-piezoelectrically driven micromixer built on paper for microfluids mixing, Biomed. Microdevices 22 (2020) 47, https://doi.org/10.1007/s10544-020-00502-7.
[36] V. Surendran, T. Chiulli, S. Manoharan, S. Knisley, M. Packirisamy, A. Chandrasekaran, Acoustofluidic micromixing enabled hybrid integrated colorimetric sensing, for rapid point-of-care measurement of salivary potassium, Biosensors 9 (2019) 73, https://doi.org/10.3390/bios9020073.
[37] G. Liu, M. Wang, P. Li, X. Sun, L. Dong, P. Li, A micromixer driven by two valveless piezoelectric pumps with multi-stage mixing characteristics, Sensors Actuators A Phys. 333 (2022) 113225, https://doi.org/10.1016/j.sna.2021.113225.
[38] Y. Huang, P.K. Das, V.R. Bhethanabotla, Surface acoustic waves in biosensing applications, Sens. Actuators Rep. 3 (2021) 100041, https://doi.org/10.1016/j.snr.2021.100041.
[39] J.Y. Lichtenberg, Y. Ling, S. Kim, Non-specific adsorption reduction methods in biosensing, Sensors 19 (2019) 2488, https://doi.org/10.3390/s19112488.
[40] B. Bachour Junior, M.R. Batistuti, A.S. Pereira, E.M. de Sousa Russo, M. Mulato, Electrochemical aptasensor for NS1 detection: towards a fast dengue biosensor, Talanta 233 (2021) 122527, https://doi.org/10.1016/j.talanta.2021.122527.
[41] D. Harpaz, N. Alkan, E. Eltzov, The incorporation of amplified metal-enhanced fluorescence in a CMOS-based biosensor increased the detection sensitivity of a DNA marker of the pathogenic fungus Colletotrichum gloeosporioides, Biosensors 10 (2020) 204, https://doi.org/10.3390/bios10120204.
[42] N. Hui, J. Wang, D. Wang, P. Wang, X. Luo, S. Lv, An ultrasensitive biosensor for prostate specific antigen detection in complex serum based on functional signal amplifier and designed peptides with both antifouling and recognizing capabilities, Biosens. Bioelectron. 200 (2022) 113921, https://doi.org/10.1016/j.bios.2021.113921.
[43] B. Somchob, N. Promphet, N. Rodthongkum, V.P. Hoven, Zwitterionic hydrogel for preserving stability and activity of oxidase enzyme for electrochemical biosensor, Talanta 270 (2024) 125510, https://doi.org/10.1016/j.talanta.2023.125510.
[44] S. Pan, H. Zhang, W. Liu, Y. Wang, W. Pang, X. Duan, Biofouling removal and protein detection using a hypersonic resonator, ACS Sensors. 2 (2017) 1175–1183, https://doi.org/10.1021/acssensors.7b00298.
[45] X. Liu, T. Zheng, C. Wang, Three-dimensional modeling and experimentation of microfluidic devices driven by surface acoustic wave, Ultrasonics 129 (2023) 106914, https://doi.org/10.1016/j.ultras.2022.106914.
[46] T. Zheng, C. Wang, C. Xu, Tritoroidal particle rings formation in open microfluidics induced by standing surface acoustic waves, Electrophoresis 41 (2020) 983–990, https://doi.org/10.1002/elps.201900361.
[47] M.F. Abd Muain, A.S. Amir Hamzah, S.L. Chia, K. Yusoff, H.N. Lim, I. Shinya, A. Ahmad Tajudin, Voltammetric-based immunosensing of Newcastle disease virus on polyethylene glycol-containing self-assembled monolayer modified gold electrode, Anal. Biochem. 697 (2025) 115700, https://doi.org/10.1016/j.ab.2024.115700.
[48] K. Petkovic-Duran, R. Manasseh, Y. Zhu, A. Ooi, Chaotic micromixing in open wells using audio-frequency acoustic microstreaming, Biotechniques 47 (2009) 827–834, https://doi.org/10.2144/000113242.
[49] N. Zainal, N. Abd Aziz, F.A. Abdul Mutalib, M.R. Buyong, Chaotic mixing of microdroplets using surface acoustic waves device, J. Adv. Res. Fluid mech, Therm. Sci. 73 (2020) 13–24, https://doi.org/10.37934/arfmts.73.1.1324.
[50] A.S. Eltaweil, E.M. Abd El-Monaem, G.M. El-Subruiti, B.M. Ali, M.M. Abd El-Latif, A.M. Omer, Graphene oxide incorporated cellulose acetate beads for efficient removal of methylene blue dye; isotherms, kinetic, mechanism and co-existing ions studies, J. Porous. Mater. 30 (2023) 607–618, https://doi.org/10.1007/s10934-022-01347-6.
[51] O.S. Bayomie, H. Kandeel, T. Shoeib, H. Yang, N. Youssef, M.M.H. El-Sayed, Novel approach for effective removal of methylene blue dye from water using fava bean peel waste, Sci. Rep. 10 (2020) 7824, https://doi.org/10.1038/s41598-020-64727-5.
[52] G. Jing, Z. Zhou, L. Song, M. Dong, Ultrasound enhanced adsorption and desorption of chromium (VI) on activated carbon and polymeric resin, Desalination 279 (2011) 423–427, https://doi.org/10.1016/j.desal.2011.06.001.
[53] P. Norouzi, M. Nezamoddini, M.R. Safarnejad, Antibody-oriented immobilization for Newcastle disease virus detection using label free electrochemical immunosensor, Chem. Pap. 75 (2021) 3061–3072, https://doi.org/10.1007/s11696-021-01546-6.
[54] OIE, Newcastle disease (infection with Newcastle disease virus), OIE Terr. Man. 2021 (2021) 1–6. https://www.woah.org/en/what-we-do/standards/codes-and-manuals/terrestrial-manual-online-access/ (accessed August 3, 2022).
[55] S. Purohit, P.K. Rao, D. Rawtani, Sampling and Analytical Techniques for COVID-19, in: COVID-19 Environ., Elsevier, 2022, pp. 75–94, https://doi.org/10.1016/B978-0-323-90272-4.00008-7.
[56] Y.Y. Broza, X. Zhou, M. Yuan, D. Qu, Y. Zheng, R. Vishinkin, M. Khatib, W. Wu, H. Haick, Disease detection with molecular biomarkers: from chemistry of body fluids to nature-inspired chemical sensors, Chem. Rev. 119 (2019) 11761–11817, https://doi.org/10.1021/acs.chemrev.9b00437.
[57] R.l. Kradin, V. Deshpande, A.J. Iafrate, General principles in the diagnosis of infection, in: diagnostic pathol, Infect. Dis. Ther. (2018) 3–15, https://doi.org/10.1016/B978-0-323-44585-6.00002-3, elsevier.
[58] S. Chakraborty, S. Nandi, K. Bhattacharyya, S. Mukherjee, Probing viscosity of co-polymer hydrogel and HeLa cell using fluorescent gold nanoclusters: fluorescence correlation spectroscopy and anisotropy decay, ChemPhysChem 21 (2020) 406–414, https://doi.org/10.1002/cphc.201901161.
[59] E. Nader, S. Skinner, M. Romana, R. Fort, N. Lemonne, N. Guillot, A. Gauthier, S. Antoine-Jonville, C. Renoux, M.-D. Hardy-Dessources, E. Stauffer, P. Joly, Y. Bertrand, P. Connes, Blood rheology: key parameters, impact on blood flow, role in sickle cell disease and effects of exercise, Front. Physiol. 10 (2019) 1–14, https://doi.org/10.3389/fphys.2019.01329.
[60] I. Jang, K.E. Berg, C.S. Henry, Viscosity measurements utilizing a fast-flow microfluidic paper-based device, Sensors Actuators B Chem. 319 (2020) 128240, https://doi.org/10.1016/j.snb.2020.128240.
[61] A. Volk, C.J. Kähler, Density model for aqueous glycerol solutions, Exp. Fluids 59 (2018) 75, https://doi.org/10.1007/s00348-018-2527-y.
[62] S. Orbay, A. Ozcelik, J. Lata, M. Kaynak, M. Wu, T.J. Huang, Mixing high-viscosity fluids via acoustically driven bubbles, J. Micromech. Microeng. 27 (2017) 015008, https://doi.org/10.1088/0960-1317/27/1/015008.
[63] H. Sakamoto, H. Kitanishi, S. Amaya, T. Saiki, Y. Utsumi, S. Suye, Development of a high-sensitive electrochemical detector with micro-stirrer driven by surface acoustic waves, Sensors Actuators B Chem. 260 (2018) 705–709, https://doi.org/10.1016/j.snb.2017.12.196.
[64] N.A. Elmaghraby, A.M. Omer, E.-R. Kenawy, M. Gaber, M.A. Hassaan, S. Ragab, I. Hossain, A. El Nemr, Electrospun cellulose acetate/activated carbon composite modified by EDTA (rC/AC-EDTA) for efficient methylene blue dye removal, Sci. Rep. 13 (2023) 9919, https://doi.org/10.1038/s41598-023-36994-5.
[65] X. Cai, S. Tan, A. Xie, M. Lin, Y. Liu, X. Zhang, Z. Lin, T. Wu, W. Mai, Conductive methyl blue-functionalized reduced graphene oxide with excellent stability and solubility in water, Mater. Res. Bull. 46 (2011) 2353–2358, https://doi.org/10.1016/j.materresbull.2011.08.039.
[66] P. Li, T.J. Huang, Applications of Acoustofluidics in bioanalytical chemistry, Anal. Chem. 91 (2019) 757–767, https://doi.org/10.1021/acs.analchem.8b03786.
[67] S.W. Ibrahim, W.G. Ali, A review on frequency tuning methods for piezoelectric energy harvesting systems, J. Renew. Sustain. Energy 4 (2012), https://doi.org/10.1063/1.4766892.
[68] C. Zhang, X. Guo, P. Brunet, M. Costalonga, L. Royon, Acoustic streaming near a sharp structure and its mixing performance characterization, Microfluid. Nanofluid. 23 (2019) 104, https://doi.org/10.1007/s10404-019-2271-5.
[69] A. Ahmad, E. Moore, Electrochemical immunosensor modified with self-assembled monolayer of 11-mercaptoundecanoic acid on gold electrodes for detection of benzo[a]pyrene in water, Analyst 137 (2012) 5839, https://doi.org/10.1039/c2an35236b.
[70] L. Blandón-Naranjo, J. Hoyos-Arbeláez, M.V. Vázquez, F. Della Pelle, D. Compagnone, NADH oxidation onto different carbon-based sensors: effect of structure and surface-oxygenated groups, J. Sensors. 2018 (2018) 1–9, https://doi.org/10.1155/2018/6525919.

[71] M.A. Pellitero, S.D. Curtis, N. Arroyo-Currás, Interrogation of electrochemical aptamer-based sensors via peak-to-peak separation in cyclic voltammetry improves the temporal stability and batch-to-batch variability in biological fluids, ACS Sensors 6 (2021) 1199–1207, https://doi.org/10.1021/acssensors.0c02455.
[72] V. Stanković, S. Đurđić, M. Ognjanović, B. Antić, K. Kalcher, J. Mutić, D. M. Stanković, Anti-human albumin monoclonal antibody immobilized on EDC-NHS functionalized carboxylic graphene/AuNPs composite as promising electrochemical HSA immunosensor, J. Electroanal. Chem. 860 (2020) 113928, https://doi.org/10.1016/j.jelechem.2020.113928.
[73] M.F. Abd Muain, K.H. Cheo, M.N. Omar, A.S. Amir Hamzah, H.N. Lim, A.B. Salleh, W.S. Tan, A. Ahmad Tajudin, Gold nanoparticle-decorated reduced-graphene oxide targeting anti hepatitis B virus core antigen, Bioelectrochemistry 122 (2018) 199–205, https://doi.org/10.1016/j.bioelechem.2018.04.004.
[74] H. Haji-Hashemi, P. Norouzi, M.R. Safarnejad, B. Larijani, M.M. Habibi, H. Raeisi, M.R. Ganjali, Sensitive electrochemical immunosensor for citrus bacterial canker disease detection using fast Fourier transformation square-wave voltammetry method, J. Electroanal. Chem. 820 (2018) 111–117, https://doi.org/10.1016/j.jelechem.2018.04.062.
[75] Y. Rasmi, X. Li, J. Khan, T. Ozer, J.R. Choi, Emerging point-of-care biosensors for rapid diagnosis of COVID-19: current progress, challenges, and future prospects, Anal. Bioanal. Chem. 413 (2021) 4137–4159, https://doi.org/10.1007/s00216-021-03377-6.
[76] G. Rong, Y. Zheng, X. Li, M. Guo, Y. Su, S. Bian, B. Dang, Y. Chen, Y. Zhang, L. Shen, H. Jin, R. Yan, L. Wen, P. Zhu, M. Sawan, A high-throughput fully automatic biosensing platform for efficient COVID-19 detection, Biosens. Bioelectron. 220 (2023) 114861, https://doi.org/10.1016/j.bios.2022.114861.
[77] T. Zheng, Y. Liu, Y. Fu, C. Wang, Asymmetrically aligned focused acoustic waves for enhancing sensing performance of electrochemical microarrays, Appl. Phys. Lett. 122 (2023), https://doi.org/10.1063/5.0147389.
[78] M. Zhou, D. Gao, Z. Yang, C. Zhou, Y. Tan, W. Wang, Y. Jiang, Streaming-enhanced, chip-based biosensor with acoustically active, biomarker-functionalized micropillars: a case study of thrombin detection, Talanta 222 (2021) 121480, https://doi.org/10.1016/j.talanta.2020.121480.
[79] F. Zhu, X. Hu, X. Wu, D. Xu, Q. Li, X. Chen, W. Pang, X. Duan, Y. Wang, M. He, Synergistic effect of acoustic streaming and nanozymes on enhanced intracellular dopamine detection, Biosens. Bioelectron. 280 (2025) 117431, https://doi.org/10.1016/j.bios.2025.117431.
[80] L. Zhang, S. Zhang, C. Floer, S.A.R. Kantubuktha, M.J.G.R. Velasco, J. Friend, Surface acoustic wave-driven enhancement of enzyme-linked immunosorbent assays: ELISAW, Anal. Chem. 96 (2024) 9676–9683, https://doi.org/10.1021/acs.analchem.4c01615.
[81] T. Quang Thinh, T. Van Vu Quan, L.B. Dương, T.H. Thuy, C.T. Xuan, M. Anh Tuan, A label-free electrochemical immunosensor for detection of Newcastle disease virus, in: V.T. Vo, T.Q. Le, H.T. Ngo, T.-H. Nguyen (Eds.), 7th Int. Conf. Dev. Biomed. Eng. Vietnam, Springer Singapore, Singapore, 2020, pp. 699–703, https://doi.org/10.1007/978-981-13-5859-3_118.
[82] P. Ji, J. Zhu, X. Li, W. Fan, Q. Liu, K. Wang, J. Zhao, Y. Sun, B. Liu, E.-M. Zhou, Q. Zhao, Fenobody and RANbody-based sandwich enzyme-linked immunosorbent assay to detect Newcastle disease virus, J. Nanobiotechnology. 18 (2020) 44, https://doi.org/10.1186/s12951-020-00598-2.
[83] J. Huang, Z. Xie, Y. Huang, L. Xie, S. Luo, Q. Fan, T. Zeng, Y. Zhang, S. Wang, M. Zhang, Z. Xie, X. Deng, Electrochemical immunosensor with cu(I)/cu(II)-chitosan-graphene nanocomposite-based signal amplification for the detection of Newcastle disease virus, Sci. Rep. 10 (2020) 13869, https://doi.org/10.1038/s41598-020-70877-3.
[84] H. Yang, Y. Xu, Q. Hou, Q. Xu, C. Ding, Magnetic antifouling material based ratiometric electrochemical biosensor for the accurate detection of CEA in clinical serum, Biosens. Bioelectron. 208 (2022) 114216, https://doi.org/10.1016/j.bios.2022.114216.
[85] D. Lee, J. Bhardwaj, J. Jang, Paper-based electrochemical immunosensor for label-free detection of multiple avian influenza virus antigens using flexible screen-printed carbon nanotube-polydimethylsiloxane electrodes, Sci. Rep. 12 (2022) 2311, https://doi.org/10.1038/s41598-022-06101-1.
[86] M. Da Silva, V. Labas, Y. Nys, S. Réhault-Godbert, Investigating proteins and proteases composing amniotic and allantoic fluids during chicken embryonic development, Poult. Sci. 96 (2017) 2931–2941, https://doi.org/10.3382/ps/pex058.
[87] Y.-R. Yun, S.Y. Lee, B. Seo, H. Kim, M.G. Shin, S. Yang, Sensitive electrochemical immunosensor to detect prohibitin 2, a potential blood cancer biomarker, Talanta 238 (2022) 123053, https://doi.org/10.1016/j.talanta.2021.123053.